



This is a repository copy of *Recycling of aluminosilicate-based solid wastes through alkali-activation: preparation, characterization, and challenges*.

White Rose Research Online URL for this paper:

<https://eprints.whiterose.ac.uk/209342/>

Version: Published Version

---

**Article:**

Feng, L., Yi, S., Zhao, S. et al. (8 more authors) (2024) Recycling of aluminosilicate-based solid wastes through alkali-activation: preparation, characterization, and challenges. *Buildings*, 14 (1). 226. ISSN 2075-5309

<https://doi.org/10.3390/buildings14010226>

---

**Reuse**

This article is distributed under the terms of the Creative Commons Attribution (CC BY) licence. This licence allows you to distribute, remix, tweak, and build upon the work, even commercially, as long as you credit the authors for the original work. More information and the full terms of the licence here:

<https://creativecommons.org/licenses/>

**Takedown**

If you consider content in White Rose Research Online to be in breach of UK law, please notify us by emailing [eprints@whiterose.ac.uk](mailto:eprints@whiterose.ac.uk) including the URL of the record and the reason for the withdrawal request.



[eprints@whiterose.ac.uk](mailto:eprints@whiterose.ac.uk)  
<https://eprints.whiterose.ac.uk/>

Review

# Recycling of Aluminosilicate-Based Solid Wastes through Alkali-Activation: Preparation, Characterization, and Challenges

Lichao Feng <sup>1</sup>, Shengjie Yi <sup>1</sup>, Shuyuan Zhao <sup>2</sup>, Qiucheng Zhong <sup>1</sup>, Feirong Ren <sup>1</sup>, Chen Liu <sup>3</sup>, Yu Zhang <sup>3</sup>, Wenshou Wang <sup>4</sup>, Ning Xie <sup>4</sup>, Zhenming Li <sup>5,\*</sup>  and Na Cui <sup>4,\*</sup>

<sup>1</sup> Jiangsu Marine Resources Development Research Institute and School of Mechanical Engineering, Jiangsu Ocean University, Lianyungang 222005, China

<sup>2</sup> National Key Laboratory of Science and Technology on Advanced Composites in Special Environments, Harbin Institute of Technology, Harbin 150080, China

<sup>3</sup> Department of Materials and Environment (Microlab), Faculty of Civil Engineering and Geoscience, Delft University of Technology, 2628 CD Delft, The Netherlands

<sup>4</sup> School of Civil Engineering and Architecture, University of Jinan, Jinan 250022, China

<sup>5</sup> Department of Materials Science and Engineering, The University of Sheffield, Sheffield S10 2TN, UK

\* Correspondence: zhenming.li@sheffield.ac.uk (Z.L.); cea\_cuin@ujn.edu.cn (N.C.)

**Abstract:** Recycling aluminosilicate-based solid wastes is imperative to realize the sustainable development of constructions. By using alkali activation technology, aluminosilicate-based solid wastes, such as furnace slag, fly ash, red mud, and most of the bio-ashes, can be turned into alternative binder materials to Portland cement to reduce the carbon footprint of the construction and maintenance activities of concrete structures. In this paper, the chemistry involved in the formation of alkali-activated materials (AAMs) and the influential factors of their properties are briefly reviewed. The commonly used methods, including X-ray diffraction (XRD), scanning electron microscopy (SEM), thermogravimetric analysis (TG), nuclear magnetic resonance spectroscopy (NMR), and X-ray pair distribution function technology, to characterize the microstructure of AAMs are introduced. Typical characterization results of AAMs are shown and the limitations of each method are discussed. The main challenges, such as shrinkage, creep, efflorescence, carbonation, alkali-silica reaction, and chloride ingress, to conquer for a wider application of AAMs are reviewed. It is shown that several performances of AAMs under certain circumstances seem to be less satisfactory than traditional portland cement systems. Existing strategies to improve these performances are reviewed, and recommendations for future studies are given.

**Keywords:** slag; fly ash; alkali-activation; microstructure; performance; challenges



**Citation:** Feng, L.; Yi, S.; Zhao, S.; Zhong, Q.; Ren, F.; Liu, C.; Zhang, Y.; Wang, W.; Xie, N.; Li, Z.; et al. Recycling of Aluminosilicate-Based Solid Wastes through Alkali-Activation: Preparation, Characterization, and Challenges. *Buildings* **2024**, *14*, 226. <https://doi.org/10.3390/buildings14010226>

Academic Editor: Ramadhansyah Putra Jaya

Received: 16 October 2023

Revised: 9 December 2023

Accepted: 8 January 2024

Published: 15 January 2024



**Copyright:** © 2024 by the authors. Licensee MDPI, Basel, Switzerland. This article is an open access article distributed under the terms and conditions of the Creative Commons Attribution (CC BY) license (<https://creativecommons.org/licenses/by/4.0/>).

## 1. Introduction

Since Kuhl first obtained a new type of cementitious material by mixing ground slag powder and caustic potash in 1950, alkali-activated materials have been considered a promising candidate to replace portland cement (PC), which contributes significant carbon emission, as the binder material in concrete structures [1]. In the alkali-activated system, the main binder phase originates from the silicate or aluminosilicate components by reacting with alkaline elements to form a  $\text{Me}_2\text{O}-\text{Me}_2\text{O}_3-\text{SiO}_2-\text{H}_2\text{O}$  system.

Alkali-activated materials (AAMs) have distinctive merits compared with Portland cement. First, from the environmental perspective, the carbon emission from manufacturing alkali-activated materials, especially using aluminosilicate solid wastes as the raw materials, is far lower than from the production of portland cement [2,3]. More importantly, the reuse of aluminosilicate solid waste can significantly reduce the environmental problems resulting from landfill [3,4], air and underwater contamination [4,5], and natural resource consumption [5,6]. It was reported that the  $\text{CO}_2$  emission can be reduced by

at least 43% compared with portland cement Gomes, 2019 [7]. Second, from the property viewpoint, alkali-activated materials have outstanding early-age strength [6,8] and high-temperature resistance [8,9].

In the solid waste categories, aluminosilicate is one of the main branches from the chemical composition perspective. Although using alkali-activated aluminosilicate solid waste as binder materials has evident benefits, palpable challenges remain. For example, drying shrinkage can lead to cracking when coupled with carbonation [10]. The efflorescence problem, which originates from the carbonation of the alkali leachates, is another common phenomenon that limits the application of the alkali-activated system [11]. Most importantly, the chemical contents of the solid wastes vary from time to time depending on the providers and the resources of the raw materials. The contents of calcium, magnesium, aluminum, iron, and silicate could be in a range of 5–35%, 10–30%, 10–40%, 20–60%, and 1–40%, respectively. Furthermore, although these composing elements are similar to portland cement, the non-active nature of the solid waste cannot guarantee the final properties of the materials.

In the past few decades, although it has been well recognized that the alkali-activation technology is a promising method to activate the inert components of aluminosilicates and although the potential activation and hydration mechanisms have shed some light on developing the new innocuous treatment of various solid wastes, many challenges from the perspectives of technology, environment, and policies still exist. First, due to the significant fluctuation and instability of the chemical composition of the raw materials, the pretreatment cost remains at a relatively high level if the final quality of the cementitious materials needs to be well controlled. As a consequence, the leverage between the property and the cost of solid waste-based cementitious materials needs to be further improved. Additionally, despite the scale effect advantage, the durability research of solid waste-based cementitious materials is still in its infancy stage, especially with exposure to an aggressive environment. Furthermore, although the solid waste-based special type of cement has been applied in some places, the problem of late-age strength reduction is still unacceptable. Second, until now, the long-term environmental impact of using recycled solid wastes as cementitious materials is still unclear. The leaching of hazardous elements, which originate from the waste, is a long-standing problem. The durability problem resulting from the mobilization of alkali elements remains challenging. The assessment of air, underground water, vegetation, and eco-systems around the solid waste-based infrastructures needs to be systematically investigated via collaboration with multi-disciplinary teams. Third, the investigation of synergistic utilization of solid wastes remains very limited. The chemical compositional variation and low activity of solid wastes significantly confined their recycling efficiency. Therefore, finding the balance between diverse industrial solid wastes through mixture design is an essential factor in obtaining a stable building material.

To solve the above-mentioned problems, it is imperative to understand the background and knowledge gap of the chemical reaction and performances of these systems, to build a bridge to connect chemical engineering, materials science, and civil engineering and thus expand the practical applications of these systems. This review article tries to provide a summary of the knowledge gaps in the chemical background, manufacturing process, microstructure characterization, and existing challenges of using alkali-activated aluminosilicate wastes as the building binder materials. The main contents of this review article will not only shed light on future research trends from an academic perspective but also provide practical supporting information in construction fields.

## 2. Chemistry of Alkali-Activated Materials

The alkali-activation of aluminosilicate can be divided into two categories, namely the alkali element activation and the alkaline earth element activation. As demonstrated in Table 1, the most commonly used caustic alkali element activators are NaOH and KOH [12,13], and the alkaline earth elements are  $\text{Ca}(\text{OH})_2$  and  $\text{Mg}(\text{OH})_2$ , which might be obtained from the active CaO or MgO from the furnace slag [14,15], and other solid wastes, such as acetylene

sludge (mainly composed of  $\text{Ca}(\text{OH})_2$ ) [16]. Apart from these base chemicals, a few weak acid salts, including  $\text{Na}_2\text{CO}_3$  [17],  $\text{K}_2\text{CO}_3$  [18],  $\text{Na}_3\text{PO}_4$  [19],  $\text{K}_3\text{PO}_4$ ,  $\text{Na-COOH}$ ,  $\text{K-COOH}$ ,  $\text{Na-COOH-CH}_2$ , and  $\text{K-COOH-CH}_2$ , can also be used as activators due to their innate basic hydrolysis reaction. In addition, water glass ( $\text{Na}_2\text{O} \cdot x\text{SiO}_2 \cdot y\text{H}_2\text{O}$ ) is another widely used activator for aluminosilicate solid waste binder materials [20]. In most cases, it was combined with  $\text{Na}_2\text{CO}_3$  and  $\text{NaOH}$  to obtain high-performance products [21].

**Table 1.** A summary of activators currently used in the related literature.

Type of Aluminosilicate Solid Waste	Activators	Reference
Rice husk ash, metakaolin	$\text{NaOH}$ and $\text{KOH}$	[12,13]
Blast furnace slag	$\text{Mg}(\text{OH})_2$ (from the active $\text{MgO}$ )	[14]
Oil fuel ash and ground blast furnace slag	$\text{NaOH}$ and $\text{Na}_2\text{SiO}_3$ [15]	[15]
Acetylene sludge, fly ash	$\text{Ca}(\text{OH})_2$	[16]
Slag	$\text{Na}_2\text{CO}_3$	[17]
Blast furnace slag	$\text{K}_2\text{CO}_3$ , coffee husk ash	[18]
Blast furnace Slag	$\text{Na}_3\text{PO}_4$	[19]
Blast furnace slag	Water glass; water glass was combined with $\text{Na}_2\text{CO}_3$ and $\text{NaOH}$	[20]
Blast furnace slag	$\text{NaOH}$ and $\text{Na}_2\text{CO}_3$	[21]

The chemical reaction between the alkali and the aluminosilicate, which governs the microstructure evolution and the final properties of the products, significantly depends on several factors, including the chemical composition of the raw materials [22], the curing temperature [23], the curing humidity [24], the curing method [25], and chemical additives [26]. It was claimed that the chemical reaction between the alkaline activators and the aluminosilicates can be divided into two types, namely the high-calcium/magnesium systems and the low-calcium/magnesium systems (as shown in Figure 1). In a high-calcium/magnesium system, the hydration product has been widely written as  $\text{C}(\text{M})\text{-A-S-H}$  which represents the calcium/magnesium aluminosilicate hydrates, typically as a Q2 layered structure, while in a low-calcium/magnesium system, the aluminum and silicon sites are coordinated and form a tetrahedral structure, i.e., mainly Q3 or Q4. In the Q4 structure, the negatively charged tetrahedral aluminum silicon coordination will be balanced by the positively charged alkaline ions to form a 3D gel structure. The specific amounts of Q1, Q2, Q3, and Q4 structures depend on the  $\text{Si}/\text{Al}$  ratio [27] and the reaction environment.

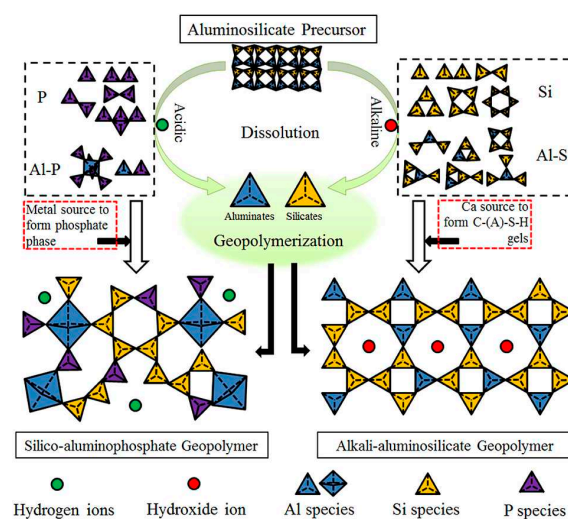


**Figure 1.** Process and reaction products of alkaline activation of a solid aluminosilicate precursor [28].

Figure 2 gives the tobermorite-like structure of the C-A-S-H gel. It can be seen that the C-A-S-H has a sandwich structure of two CaO layers with a tetrahedral silicate layer in the middle. Although it can be found that part of the silicon position can be replaced by aluminum to form a bridge site that connects the whole chain of the C-A-S-H gel, the substitution of the silicon site by aluminum is a key element of the C-A-S-H chain structure and the replacement rate is lower than 20% depending on the cross-linking degree. Similarly, the calcium sites replaced by magnesium are also limited because the ionic radius of  $Mg^{2+}$  is at a mismatch with the tobermorite structure [29].

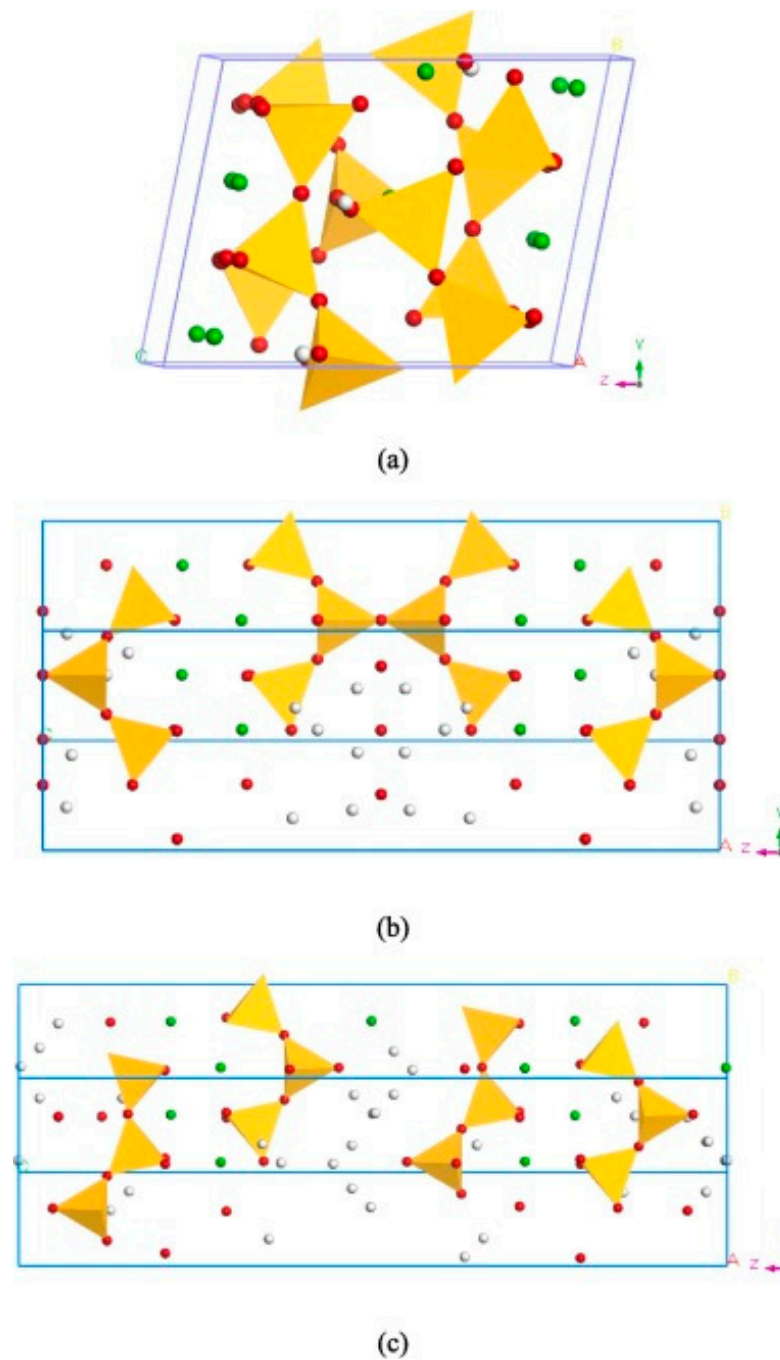


**Figure 2.** The tobermorite-like C-A-S-H gel structure, (a) tobermorite 9 Å, (b) tobermorite 11 Å, and (c) tobermorite 14 Å (color legend: hydrogen H (white); calcium Ca (green); oxygen O (red); silica Si (yellow polyhedra) [29].

### 3. Precursor Compositions, Activators, and Curing

Typical aluminosilicate solid wastes are mainly the by-products of industrial or agricultural production, such as blast furnace slag, steel slag (Figure 3), fly ash, red mud (Figure 4), various types of sludge, waste glass powder, and agricultural biomass ashes. As solid wastes, these aluminosilicates are neither stable in chemical composition nor consistent in pozzolanic activity [10,11]. As a result, it is impossible to control the properties of the final products using a universal or fixed manufacturing method. In most cases, different solid wastes need specific mix designs, curing conditions, and activators to achieve the desired properties.

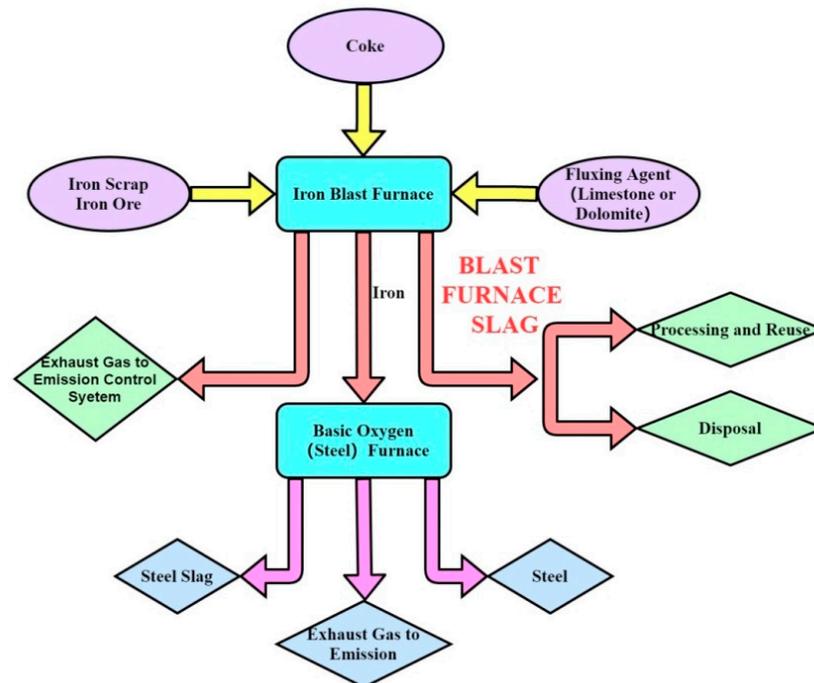


**Figure 3.** Steel slag is a by-product of iron ore.

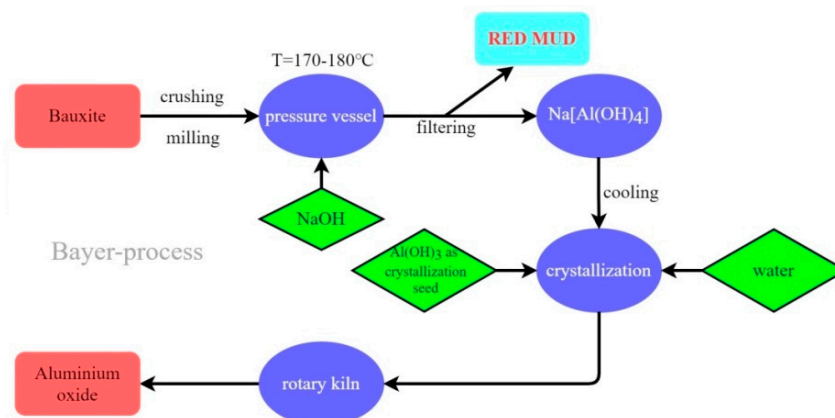


**Figure 4.** The process of preparing aluminum oxide from bauxite.

#### 3.1. Chemical Compositions of Precursors

One of the determinant factors for alkali-activated solid waste cementitious materials is the chemical composition of the raw materials. In this system, the ratio between the Si/Al/alkali elements/water determines the microstructure and properties of the final products (Figure 5) [30,31]. In a red mud system, it was found that the compressive strength of the samples presented an inverted V shape with an increasing ratio of Ca/(Si + Al). The highest compressive strength of the samples can reach about 25 MPa when the ratio of

Ca/(Si + Al) is about 1.0. The frost resistance testing results indicated that the minimum mass loss of these samples after 25 freeze/thaw cycles is 1.72% which is lower than the requirement of less than 5%. The microstructure analysis demonstrated that the Na<sup>+</sup> acts as a charge balance of the [AlO<sub>4</sub>]<sup>-</sup>, and the main reaction products include amorphous ettringite. The enhancement of the compressive strength and durability originated from the densification of the hydration products. With the decreasing ratio of Ca/(Si + Al), the [AlO<sub>4</sub>]<sup>-</sup> structure, relative bridge oxygen (RBO) numbers, and the amount of the ettringite in the gel networks fluctuated accordingly. The influence of amorphous gel phases on the final properties is greater than that of the ettringite [32].

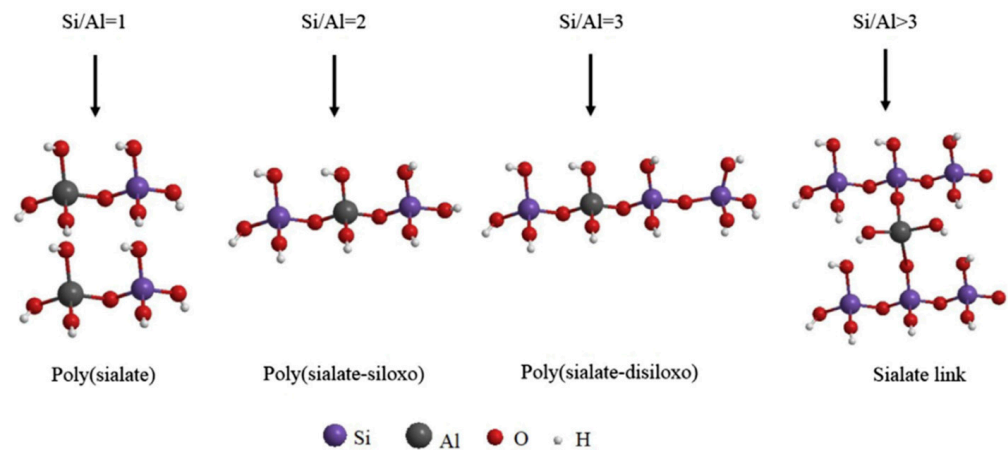


**Figure 5.** Aluminosilicate chains in aluminosilicate oligomers with various Si/Al rates [30].

Although the above-mentioned study gave an example of how the ratio between Ca and Si/Al affects the microstructure and properties of the samples, the impact of the Si/Al ratio on the alkali-activated aluminosilicate solid wastes was not discussed. To further demonstrate the impact of the Si/Al ratio on the microstructure evolution and the mechanical properties, the authors explored a fly ash system with various ratios of Si/Al. Similar to previous studies, it was reported that the mechanical properties and the efflorescence of the activated materials fluctuated with an increasing Si/Al ratio. The highest performance of the samples was obtained with a Si/Al ratio of 1.5. Under this condition, the average pore volume and pore size can reach 0.017 cm<sup>3</sup>/g and 6.21 nm, respectively, and the [AlO<sub>4</sub>]<sup>-</sup> structure content reaches the highest amount [33].

### 3.2. Activators

Blast furnace slag is the earliest one that has been used as a potential cementitious material. Blast furnace slag can be activated slowly by water due to the high content of active CaO and MgO. The main chemical composition of blast furnace slag can be written as  $x\text{CaO}/\text{MgO}-y\text{Al}_2\text{O}_3-z\text{SiO}_2$ . A few impurity elements, such as titanium, manganese, sulfur, or phosphorus are also included in minor proportions, depending on the location of the iron ore mining. The chemical composition, mainly represented by the Ca(Na)/Al/Si ratio, is the critical factor that governs the final properties of the alkali-activated furnace slags [10,15,17,19]. It was reported that the compressive and flexural strength were considerably enhanced with increasing SiO<sub>2</sub>/Al<sub>2</sub>O<sub>3</sub> and Na<sub>2</sub>O/SiO<sub>2</sub>. The optimized ratios were SiO<sub>2</sub>/Al<sub>2</sub>O<sub>3</sub> = 2.75, Na<sub>2</sub>O/SiO<sub>2</sub> = 0.25, and H<sub>2</sub>O/Al<sub>2</sub>O<sub>3</sub> = 13 [34].

In all conditions that determine the properties of the alkali-activated furnace slag, the types and modules of the activator are the decisive factors. In most cases, NaOH and water glass (Na<sub>2</sub>O•xSiO<sub>2</sub>•yH<sub>2</sub>O) can act as suitable activators to manufacture the alkali-activated furnace slag. It was found that by using potassium hydroxide-silicate (with a modulus of 1.25) as the activator, the slag system can be successfully activated as cementitious material. It was claimed that the calcium in slag considerably governs the early- and late-age properties, and the free calcium ions enhance the formation of the

geopolymer gel. It was argued that the hardening process is derived from the C-A-S-H precipitation and the accelerated geopolymerization [35].

Apart from water glass and alkali hydroxides, a few weak acid salts, such as  $\text{Na}_2\text{CO}_3$ , are feasible to act as supplementary activators by combining them with water glass and NaOH. In addition, industrial glass waste was also considered an activator that can be used to manufacture alkali-activated slag. Although the authors stated that industrial glass waste is an effective activator for the slag system, the enhancement of the mechanical properties originated from the dissolution of the Si in the waste glass by treating it with NaOH/ $\text{Na}_2\text{CO}_3$ . Microstructure analysis revealed that the mechanical properties and the nanostructure were governed by the Si/Na ratio [36].

Disagreeing with Puertas' point of view about the NaOH/ $\text{Na}_2\text{CO}_3$  activation system, Jeon's study claimed that the benefits of the  $\text{Na}_2\text{CO}_3$  in the NaOH system are very limited. Instead of NaOH, it was stated that the  $\text{Na}_2\text{CO}_3$  has a noticeable activation effect on the  $\text{Ca}(\text{OH})_2$ -activated fly ash system. The strength of the  $\text{Ca}(\text{OH})_2$ -fly ash system can be improved over 4–5 times with the addition of a small amount of  $\text{Na}_2\text{CO}_3$ . The microstructure analysis demonstrated that the main reaction product is C-S-H instead of a geopolymer gel.  $^{27}\text{Al}$  NMR results indicated that the addition of  $\text{Na}_2\text{CO}_3$  is beneficial to the substantial release of Al from the fly ash. In addition, the SEM results demonstrated that the addition of  $\text{Na}_2\text{CO}_3$  resulted in a dense hardened matrix and left fewer unreacted fly ash particles. Although the potential mechanism of the porosity change was not provided, the authors tested the pore size and porosity and pointed out that the pore size and porosity can be significantly reduced by combining the fly ash with  $\text{Na}_2\text{CO}_3$  [37].

Different from alkali/alkaline earth hydroxides or water glass, both CaO and MgO can also serve as activators. Compared with  $\text{Ca}(\text{OH})_2$ , CaO shows a more effective activation capability in the furnace slag system. The 28 days compressive strengths of the CaO- and  $\text{Ca}(\text{OH})_2$ -activated pastes are 42 MPa and 23 MPa, respectively. Microstructure analysis demonstrates that more C-S-H phases are formed by using CaO than by using  $\text{Ca}(\text{OH})_2$ , and the carbonation effect is far lower in the CaO system [38]. Another study demonstrated that a mixture of MgO and NaOH with a proportion of 1:1 can activate the furnace slag effectively. With a mass ratio of 4, 6, and 8% of the slag, the highest 90-day compressive strength can reach 54 MPa cured at 20 °C. The microstructure analysis of the paste, including backscattering SEM and solid-state  $^{27}\text{Al}$  and  $^{29}\text{Si}$  MAS NMR spectroscopy, shows that dense C-A-S-H is the main binder phase, and that hydrotalcite-like phases and third aluminate calcium hydrate can be detected [39].

In addition to specifically manufactured alkali hydroxides, water glass, or Ca/Mg oxides, synergistically using strong alkali solid wastes as activators is a promising eco-friendly method to manufacture low-carbon alkali-activated green cementitious materials [40–42]. A recent study gave an example that using soda sludge as an activator to manufacture alkali-activated cementitious material with blast furnace slag. Since the soda sludge contained a high amount of  $\text{Ca}(\text{OH})_2$ , the dissolution of  $\text{Ca}(\text{OH})_2$  increased the pH values of the pastes and promoted the dissolution of the slag. The mixtures could be further optimized by introducing industrial gypsum to tailor the reaction products with more ettringite formation [40]. Wastes containing soluble alkali salts or soluble silicates as part of a hybrid activator can be another option. One of the cases is the use of air pollution control (APC) residues rich in NaCl and  $\text{Na}_2\text{SO}_4$  reported as activators when combined with sodium silicates for slag and waste glass powder activation. Secondary reaction products such as ettringite and Friedel's salt could be formed that contribute to the strength development [41]. Waste-derived sodium silicates from rice husk ash and NaOH pellets were reported as the activators that could achieve a comparable structural build-up, but the residuals of rice husk ash could negatively affect the mechanical properties of the geopolymer [42].

### 3.3. Curing Conditions

In addition to activators, the curing condition is another critical factor that determines the properties of the alkali-activated aluminosilicates. Except for traditional heat and

humidity curing, microwave curing has been considered an effective method to mitigate the thermal gradient problem during the curing process. Compared with traditional heat and humidity curing, the alkali-activated fly ash mortar after microwave curing demonstrates a faster property development (Figure 6). It was claimed that the compressive strength of the samples after 120 min microwave curing at an average incident power of 240 W has comparable values to samples cured for 48 h at 75 °C. Especially for the samples activated by 10 M NaOH, the compressive strength of microwave curing can reach about 60 MPa which is over 30% higher compared with the traditional curing of samples. It was also stated that the microstructure of the hydration products is denser than that of traditionally cured ones and this results in a higher compressive strength. Furthermore, it was found that the compressive strength is proportional to the energy absorption from microwave radiation [43].

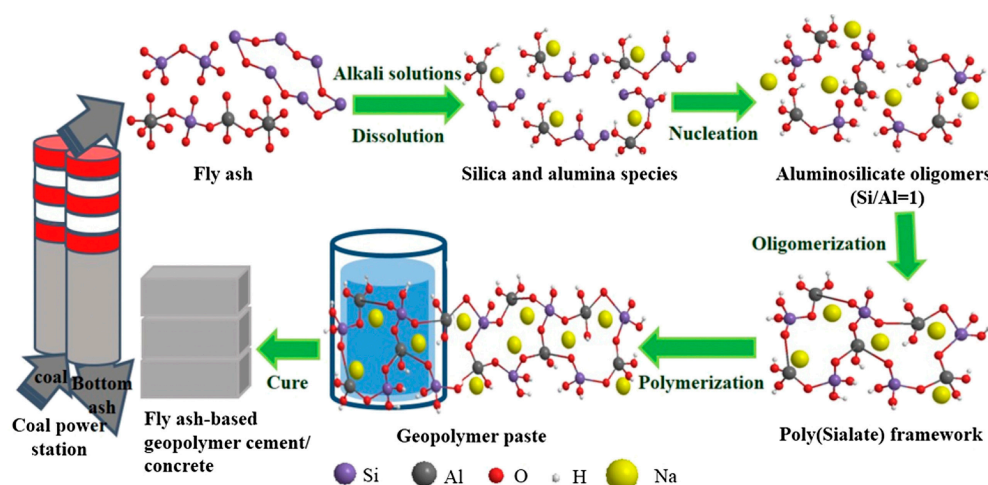


Figure 6. Process from fly ash to fly ash-based alkaline-activated cementitious materials [30].

The pore solution and carbonation resistance of alkali-activated fly ash/slag paste with sealed or unsealed curing conditions were compared. For unsealed samples, they were cured in a fog environment at room temperature with a humidity of 99% for 28 days. The atmosphere was normal air with 400 ppm CO<sub>2</sub>, and the sealed samples were not removed from the curing jar until day 28. The unsealed curing samples have a few counter-activated mechanisms. First, it was claimed that the unsealed curing samples have an inward movement of the ions from the surface to the interior of the samples due to the humidity difference between the environment and the samples. Second, the condensation of the water on the surface of the samples leads to an outward movement of the ions due to the difference in the ion concentrations. In that study, it was reported that the ions moving outwards is the main mechanism that accounts for the alkali leaching phenomenon. In addition, the leaching resulted in the carbonation process, and the replacement of the fly ash by the furnace slag has a considerable benefit for the carbonization resistance. It was found that the sealed curing samples showed a better long-term performance in light of the carbonization resistance and the late-age gel formation perspective [44].

It was found that thermal activation could be beneficial for the strength development of AAMs since it can accelerate the geopolymerization process; however, temperatures above certain degrees could bring side effects, as reported by Ana Balaguer Pascual who showed that geopolymers prepared with waste glass and metakaolin showed a strength loss when the temperature was at 80 °C. Meanwhile, it is essential to consider this from both the properties of geopolymer as well as from the economic point of view as the thermal curing process is highly energy demanding [45].

## 4. Microstructure Characterization Methods

### 4.1. X-ray Diffraction (XRD)

XRD is a commonly used characterization method in cementitious materials. Since minerals have distinct diffraction patterns, XRD could be applied to determine the mineralogical changes in precursors and possibly hydrated minerals before and after alkali-activation. For aluminosilicate-based industrial wastes, there are not only glass phases but also a variety of mineral phases. The reactions between mineral phases and activators can be told according to the phase change detected using XRD. Examples such as feldspar minerals dissolving in an alkaline solution to form geopolymer gels are reported by [46]. Meanwhile, crystalline hydration products such as hydrotalcite in alkali-activated slag and zeolite in metakaolin/fly ash-based geopolymers can also be verified from the XRD patterns [47,48].

In addition to the qualitative determination of the minerals, the Rietveld refinement of XRD results can be further applied to conduct quantitative analyses. In AAMs, the primary reaction products are N-A-S-H gels and C-(A)-S-H gels, as well as the coexistence of different gels [49,50]. Due to the semi-crystalline nature of these gels, in most cases, there will only be a broad hump ranging from 20 to 30 degrees of 2 theta that can be observed in the XRD patterns. For this reason, it is difficult to distinguish the exact type of gels using XRD results alone. An example is illustrated in Figure 7. Moreover, the intensity of peaks can also be affected by the glass phases from the aluminosilicates' amorphous phases that may have the same broad diffraction hump. Coupling this with partial or no known crystal structure (PONKCS) methods, it is possible to quantify the number of amorphous phases in the AAMs and determine the reaction degree of the precursors in the form of the amorphous phases [51,52].

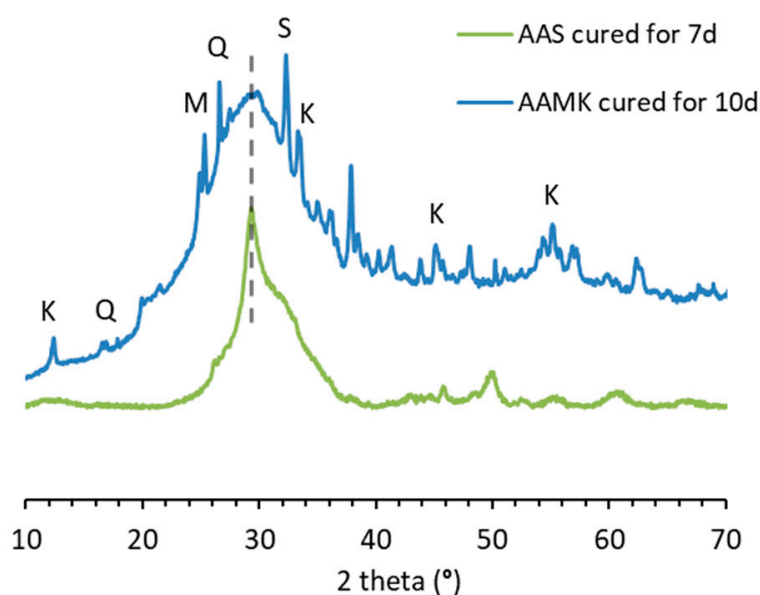


**Figure 7.** XRD patterns of alkali-activated slag (AAS) and alkali-activated metakaolin (AAMK), as typical examples of high- and low-calcium AAM systems, respectively. K, M, Q, and S represent kaolinite, mullite, quartz, and sodium carbonate, respectively. The dashed line indicates the main band of C-(A)-S-H gel. The data for AAS and AAMK are from [53] and [47], respectively, and were collected by the same author; thus, are comparable.

While XRD is known to be sensitive to crystalline phases, a prerequisite is that the size of the lattice phase is large enough. Nano-crystals, e.g., those in a length scale of around 5 nm, are detectable using electron diffraction experiments but not using XRD [54].

#### 4.2. SEM/EDS

Scanning electron microscopy (SEM) is an important tool to study the microstructure of materials. SEM makes it possible to visualize the morphology of the materials at the microscale. Due to the low conductivity of the AAM samples, the materials usually need to be coated with carbon or gold first to avoid charging samples and to obtain a better view of the images.

Secondary electrons (SE) are normally used to observe the fracture surface of the AAM samples, as they can give information on the surface topography morphology of the materials. The morphology of the precursors as well as the reaction products can be viewed. With the implement of SE analysis, a general view of how microstructure gets developed and how the gels and unreacted particles are bonded can be observed. An example of AAMs made from different industrial wastes is shown in Figure 8 [55].

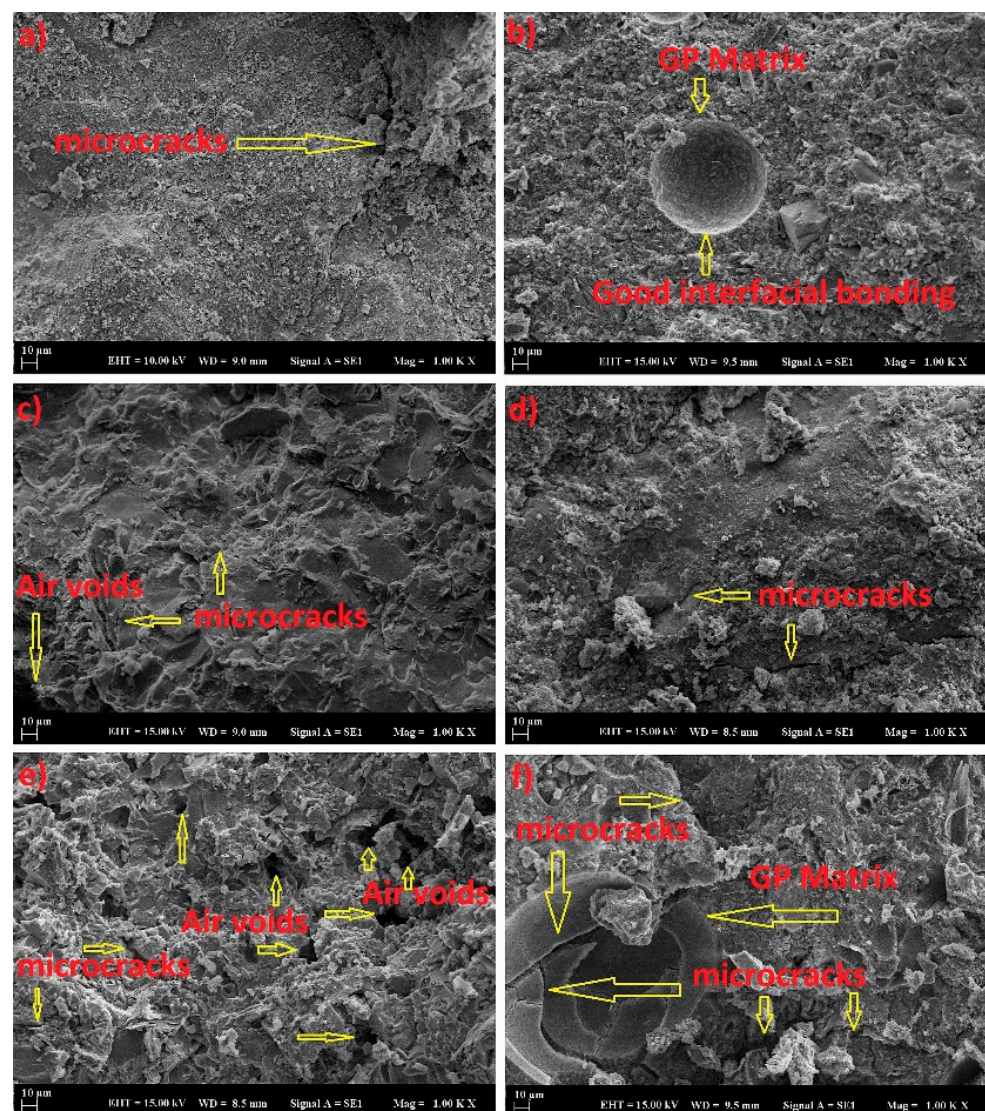


**Figure 8.** SEM images of different types of waste-derived AAMs (waste marble powder (MP), waste brick powder (BP), ceramic waste powder (CW), waste glass powder (GP), and rice husk ash (RHA)); 75CW1,6 (a), 25BP1,3 (b), 50RHA1,6 (c), 25MP1,2 (d), 50GP1,2 (e), and 100RC1,1 (f) [56].

Backscattered electrons (BSEs) are another type of electrons used in SEM. An example is shown in Figure 9. One of the most interesting characteristics of BSEs is that the brightness of the image is dependent on the average atomic numbers. A brighter spot indicates a

larger average atomic number. Therefore, this technique can be used to separate different phases in the AAMs after reactions. To better distinguish the phases, samples should be well-polished. Based on the brightness of different phases, it is possible to study the hydration degree of the precursors, and even determine the pore size distribution of the AAM matrix, see Figure 10 [57].

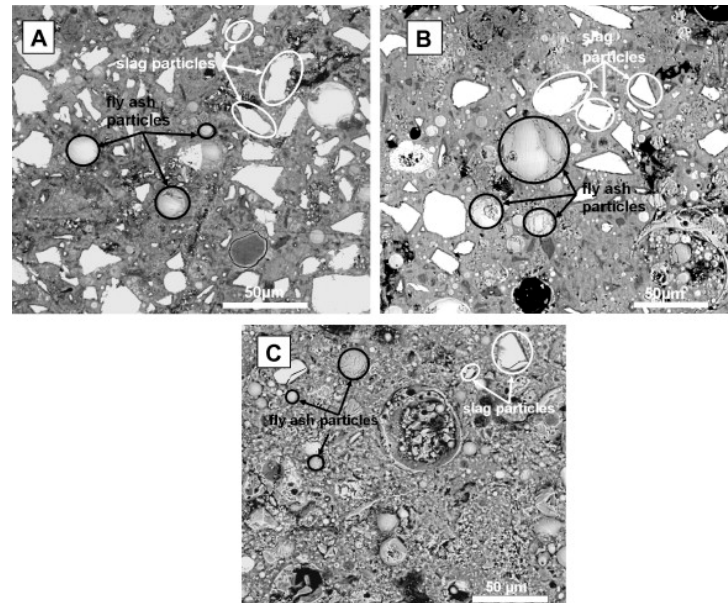


**Figure 9.** BSE images of alkali-activated blended binders after 28 days of curing (A) 75 wt.% slag/25 wt.% fly ash, (B) 50 wt.% slag/50 wt.% fly ash and (C) 25 wt.% slag/75 wt.% fly ash [58].

Apart from the image analysis, with the coupling of energy-dispersive spectroscopy (EDS), further analysis can be focused not only on morphology but elemental compositions. The chemical compositions of the reaction products, especially the gel compositions in AAMs, can be determined from this point. Research on this perspective has been intensively investigated and the gels' compositions were associated with the mechanical properties and durability of the AAMs [59]. A general summary of the gel compositions in AAMs is shown in Figure 11 with the Al-Si-Ca element ratio presented in the ternary diagram.

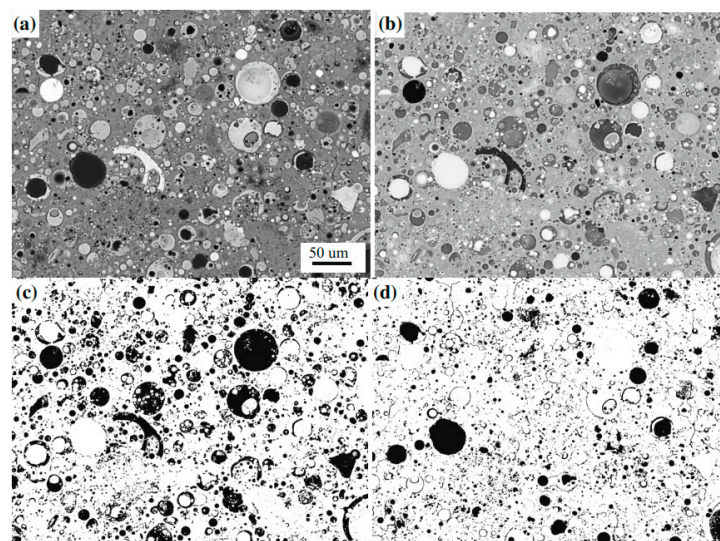


**Figure 10.** Images after different segmentation steps. (a) Original image; (b) invert image; (c) binary image of unreacted fly ash; (d) binary image of pores [57].

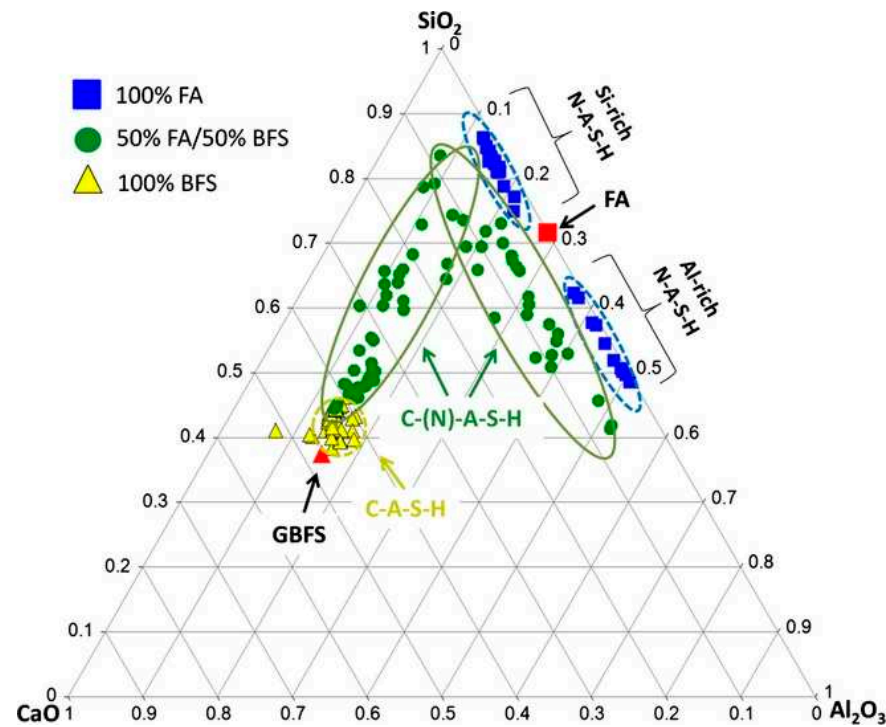


**Figure 11.** Pseudo-ternary plot of alkali-activated binder gel compositions, measured using SEM–EDX after 28 d of curing. Binders are synthesized by sodium metasilicate activation of fly ash (FA), slag (BFS), and a 1:1 mixture of these two precursors [60].

While it seems that all AAMs can be observed using SEM under different modes, attention needs to be paid when using the function of EDS. During the work of electron microscopy, the electrons released by the instrument experience a series of elastic and inelastic collisions with atoms of the material on the surface. The volume in which these collisions occur is considered the ‘interaction volume’. The higher the accelerating voltage, the larger the interaction volume [61]. When analyzing the elemental compositions of phases with a small size, e.g., the rim around unhydrated slag grain, a high accelerating voltage can contribute to the formation of a large interaction volume including interference of surrounding phases, leading to the generation of inaccurate information [56].

#### 4.3. TG-DTG

Thermogravimetric analysis (TGA) is a method for measuring the weight loss of samples at elevated temperatures. During the heating process, the mineral phases and reaction products in AAMs undergo thermal decompositions, resulting in weight loss due to the loss of water or carbonates from the products (Figure 12). It is possible to quantify the amount of bound water in AAMs and, to a certain extent, the reaction degree of precursors. In the meantime, the various mineral phases and gels have distinct decomposition temperature ranges, making it easy to compare the quantities of the various phases. To accomplish this, differential thermogravimetric analysis (DTG) is frequently used, as it can provide more accurate decomposition ranges for the individual phases. In AAMs, the weight loss is mainly located in temperatures ranging from 100 to 120 °C, as the consequence of dehydration of the geopolymer gels. The minerals such as hydrotalcite show the decomposition with the doublet peak within the temperature ranges of 200–400 °C.

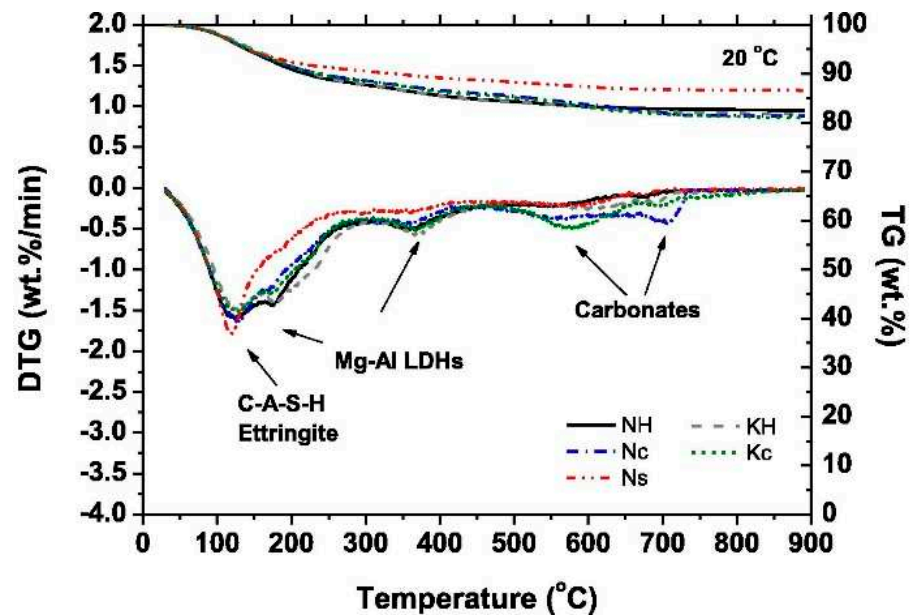


**Figure 12.** TG–DTG curves of alkali-activated slag. NH, KH, Nc, Kc, and Ns represent the activator type of NaOH, KOH, Na<sub>2</sub>CO<sub>3</sub>, K<sub>2</sub>CO<sub>3</sub>, and Na<sub>2</sub>SO<sub>4</sub>, respectively [62].

Compared with XRD measurements, TG is sensitive towards X-ray amorphous materials, e.g., the C-A-S-H gel phase. However, one should keep in mind that the TG-DTG results depend heavily on many factors, such as the heating rate, properties of the vessel, sample weight, particle size of the sample, etc. Therefore, it is suggested to stick as much as possible to the same procedure for all measurements [63]. Additionally, in AAM systems, the decomposition peaks of hydrates often overlap with each other. For example, the C-A-S-H gel phase, the main product of slag-based AAMs, actually shows weight loss over a broad temperature range, up to ~600 °C [49]. In this range, most other hydrates decompose, including carbonate phases. Thus, the quantification of different phases in AAMs using TG-DTG alone is difficult, and the combination with other techniques mentioned in this section should be a good option.

#### 4.4. Nuclear Magnetic Resonance (NMR)

NMR is a powerful tool that has been used for cementitious materials for about 40 years [64]. The chemical environment and connectivity of certain elements such as Si, Al, Na, and H in raw materials as well as reaction products can be elaborated with this method in detail. In terms of studies on AAMs, this technique also achieves great success in understanding precursors, the kinetics of polymerization, and degradation mechanisms.

The typical <sup>29</sup>Si MAS NMR spectra of slag, fly ash, and metakaolin, the three main precursors widely used in AAMs, are shown in Figure 13. Q0 and Q1 are the main two chemical coordination states of Si in slag which is a calcium silicate-based material, while Q3 and Q4 are the main two states of Si in fly ash and metakaolin which are aluminosilicate-based materials. The NMR results indicate that the polymerization degree of fly ash and metakaolin is higher than that of slag. Normally, the reactivity of calcium aluminosilicate glasses is strongly dependent on the connectivity of the network and thus the chemical composition. Si and Al are normally the network formers while Ca and Na are charge compensators as well as network modifiers in the precursor. The presence of alkaline and alkaline earth ions like (Na, K, Ca, and Mg) can enhance the reactivity of materials [65].

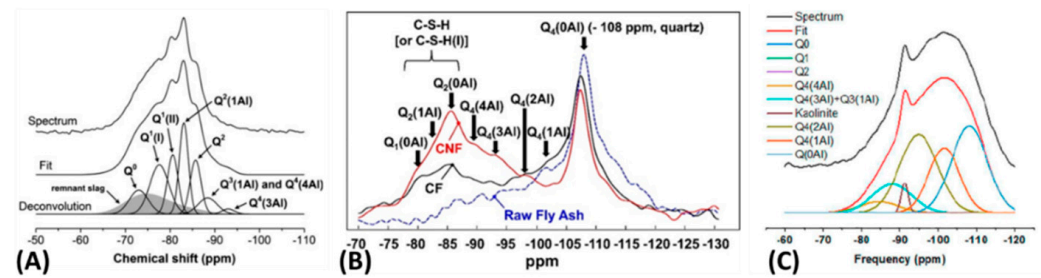


**Figure 13.** Deconvoluted  $^{29}\text{Si}$  MAS NMR spectrum of (A) slag [66], (B) fly ash [37], and (C) metakaolin [47].

Figure 14 shows the  $^{29}\text{Si}$  MAS NMR and  $^{27}\text{Al}$  MAS NMR spectra of sodium silicate-based alkali-activated slag-based pastes. It can be seen that the chemical state of Si is dominated by Q1, Q2, and Q2(1Al) at about  $-80$  ppm,  $-83$  ppm, and  $-86$  ppm, respectively. In the meantime, a tiny amount of peak located at  $-91$  ppm is detected as well, which is assigned to the Q3(1Al) in the C-(N)-A-S-H gels. In AAS paste (right one of Figure 14), Al(IV) ( $50$ – $80$  ppm) and Al(VI) ( $0$ – $20$  ppm) are detected. The formation of the main peak of Al(IV) and a small shoulder on the high-frequency part are related to the dissolution of slag and the formation of gels. Al(VI) represents the Al in hydroxalite and part of the Al octahedron near the interlayer of the gels [67]. With the reaction of time, there is no evident change in the chemical environment of Si and Al. However, a decreasing trend of the mean chain length of the gel, which can be calculated from the fraction of different Si sites, is found.

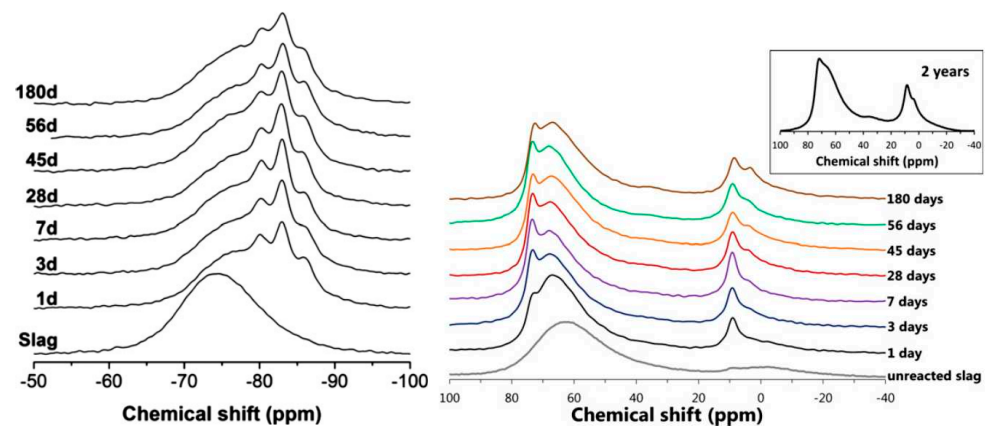


**Figure 14.**  $^{29}\text{Si}$  MAS NMR (left) and  $^{27}\text{Al}$  MAS NMR spectra (right) of sodium silicate-based slag paste cured for 180 days [66].

NMR is also applied to investigate the various degradation mechanisms in AAMs including carbonation [50], acid resistance [68], sulfate resistance [69], leaching, and e-florescence [70]. The limitations of this technique are also evident. For example,  $^{43}\text{Ca}$  is a moderately sensitivity nucleus but with an extremely low natural abundance, limiting the intensity of the signal in NMR measurement. Additionally, magnetic materials are not allowed to be tested, which limits the utilization of this technique in AAMs based on iron-containing ashes.

#### 4.5. PDF

The X-ray pair distribution function (PDF) is a promising technique to characterize the amorphous binder phases in cementitious materials. Although this characterization technique significantly depends on the testing equipment, it is still a promising approach to understanding the atomic structure of the amorphous materials on the nanoscale. The PDF method combines the X-rays from synchrotron sources and advanced detectors to give

a high real-space resolution of long-range disordered materials. By collecting the scattered X-ray data after correction, including background and detector geometry, the X-ray pair distribution function,  $G(r)$ , can be generated by a Fourier transformation process. It gives the probability of any two atoms as a function of interatomic distance [71–73].

The phase formation of the NaOH-activated GGBS pastes has been investigated through the PDF analysis. Unlike the reciprocal space analysis, in which the microstructure of the secondary reaction products is similar, the PDF analysis indicates a distinctive difference in the main calcium–sodium aluminosilicate hydrate (C-(N)-A-S-H) gel phase in a short-range atomic order. The results reveal that calcium is critical in the silicate-rich phases to form various chemical compositions on a nanoscale, determining the final properties of the activated GGBS [71]. By using the PDF analysis, White [72] stated that after 90-day curing, the initially formed gel structure is transformed to a more stable and more ordered state through the accrual of cross-linking in the geopolymer gel. It was also claimed that the activator types are critical factors corresponding to various aluminosilicate precursors. Metakaolin with a layered structure is different from fly ash with a spherical structure [73].

## 5. Challenges and Future Trends

It has been known that AAMs can show superior properties to PC systems in some aspects. Slag-based AAMs, for example, usually show high mechanical properties [74], while low-calcium AAMs like fly ash or metakaolin-based geopolymers have good thermal resistance and can immobilize metal cations such as  $Pb^{2+}$ ,  $Cd^{2+}$ , and Cs [75–77]. AAMs also attracted special attention due to their capacity to encapsulate nuclear waste [78,79]. However, challenges also exist to further expand the application of these sustainable materials, especially in structural engineering. In the literature, various properties have been considered, some of which appear more problematic than for PC systems.

### 5.1. Shrinkage

AAMs, especially those based on slag, have been intensively reported to show large shrinkage in either sealed conditions, i.e., autogenous shrinkage [53], or drying conditions, i.e., drying shrinkage [80]. The shrinkage magnitude can be several times higher than that of PC systems [81].

A high content of slag in the precursor, e.g., >30%, a silicate modulus of the activator around 1.5, and a liquid-to-binder ratio lower than 0.4 can all lead to high autogenous shrinkage [82–84]. The main reason behind this lies in the denser microstructure of the matrix, which means higher internal capillary tension when self-desiccation happens, a similar mechanism as identified in PC systems. However, AAMs do hold particular mechanisms of autogenous shrinkage due to the presence of large amounts of ions in the pore solution. The sodium ions and surrounding water molecules, for example, provide repulsive steric hydration forces between the solid particles which compensate the attractive forces like the van der Waals force. During the reaction, ions are consumed and the steric hydration force decreases, thus leading to the shrinkage of the matrix [53]. Moreover, the condensation reaction between silicates was also reported to cause shrinkage of the products without the need for moisture loss or temperature change [85]. These mechanisms are not detected in PC systems. For low-calcium AAMs, like alkali-activated fly ash (AAFA), the self-desiccation is not severe since the water molecules are not consumed by polymerization forming an aluminosilicate structure [86]. Therefore, the autogenous shrinkage of these materials is usually not significant [87]. However, the consumption of ions still occurs [88] and the syneresis process has been hypothesized to cause autogenous shrinkage of the system [89].

Given the different mechanisms of autogenous shrinkage of AAMs, various mitigating strategies ought to be explored for different systems. Traditional shrinkage-reducing agents (SRA) may not work for AAMs [90–93]. For high-calcium AAMs, internal curing has been found effective in mitigating autogenous shrinkage, especially after the first days [94].

Superabsorbent polymers, lightweight aggregates, and zeolites can all provide internal curing after pre-absorption [95–97]. Other admixtures that can alter the reaction kinetics and microstructure of AAMs can also modify their shrinkage behaviors, but the development of strength can be compromised if the reaction is delayed [47,98].

When AAMs are exposed to drying, a higher shrinkage than autogenous shrinkage is always observed because the shrinkage is driven by the combination of external and internal attractive forces. The effect of moisture loss on the capillary force is similar to that identified in self-desiccation [99], but the magnitude of shrinkage is not evenly distributed in the concrete. The surface concrete shows larger shrinkage than the interior part under drying and the shrinkage gradient will cause self-restraint of the concrete [100]. Tensile stress (or so-called eigenstress) will then be generated and can induce microcracking which develops from the surface. Slag-based AAMs are very vulnerable to drying [101], partially because of the pronounced viscoelasticity of the CNASH gel [102]. Compared to C-S-H, C-(N)-A-S-H tends to show larger deformation even under the same magnitude of driving forces [53]. The local creep deformation of the gel can cause relaxation in one place, but new stress concentration in other areas, which will facilitate the propagation of microcracking [103]. The presence of microcracks is harmful to several properties of the concrete, e.g., the elastic modulus [104], although the compressive strength may not be directly affected. The cracks also act as paths for the attack of external chemicals, e.g., CO<sub>2</sub>. It has not been clarified yet whether drying shrinkage and carbonation of AAMs can enhance each other. If so, it will be a difficult issue to tackle, especially considering the possible existence of carbonation shrinkage. Elevating the curing temperature could help to reduce the shrinkage, but does not seem to be a practical solution in engineering [105].

Plastic shrinkage of AAMs has not been intensively studied, but the huge early-age drying shrinkage of slag-based AAMs already indicates the susceptibility of these materials to moisture loss. Considering also the low elastic modulus of AAS just after setting [53,85], there is no reason to doubt that the plastic shrinkage and early-age cracking of these materials can be less severe than for PC systems. Future studies should be conducted to identify effective mitigating strategies for different types of shrinkage of AAS-based systems.

### 5.2. Creep

The creep deformations of AAS and AAFA differ due to the different reaction products of these systems [106,107]. The AAS system seems to show larger creep due to probably the same reason for its large shrinkage, i.e., the pronounced viscoelasticity of the C-(N)-A-S-H gel. By contrast, the NASH gel with a 3D structure appears much more stable under load [108]. A deeper understanding of the creep mechanisms of AAMs has not yet been reached so far; unfortunately, no microstructure-based model has been proposed yet. One challenge of this topic lies in the interaction between creep and drying shrinkage of the concrete, especially the effect of microcracking on the development of creep. Effort on this issue has been made for PC-based concrete [109] but not yet for AAM systems. On the other hand, however, creep also brings benefits to structural concrete, like stress relaxation in highly stressed regions in concrete [100]. Future studies should figure out the coupled effect of creep and relaxation on alkali-activated concrete.

### 5.3. Efflorescence

Efflorescence is the “white deposit” forming on the surface of AAMs as a result of the chemical interaction between leached Na ions and atmospheric CO<sub>2</sub>. Many researchers have observed this phenomenon and investigated the influential factors of efflorescence.

Škvára et al. [110] found that Na is weakly bonded in the N-A-S-H gels and can easily leach out without significantly compromising the compressive strength. In addition, the leaching of Na is considerably mitigated if the samples are heat-treated above 600 °C. Zhang et al. [111] studied the efflorescence of fly ash-based geopolymers and reported that the extent of efflorescence is significantly dependent on the type of activators. At the same alkali dosage and curing temperature, NaOH-activated geopolymers exhibited less and

slower efflorescence than those activated by  $\text{Na}_2\text{SiO}_3$ . The addition of soluble silicate and slag reduced the efflorescence rate but had a negligible effect on the efflorescence potential.

Efflorescence is not just an aesthetic issue but also a potential structural problem. Zhang et al. [112] investigated the influence of efflorescence on the microstructure and mechanical properties of fly ash-based geopolymers. Despite the efflorescence products not affecting the phase assemblage of the surface of samples, the mechanical properties are impaired resulting from the alkali loss and sub-efflorescence. The sub-efflorescence can be regarded as an extended efflorescence that happens beneath the surface of samples. It is detrimental to the samples since the formation of crystalline carbonates generates tensile stress in the matrix and can potentially lead to microcracking.

Given the impacts of efflorescence and sub-efflorescence, intensive studies were conducted to develop mitigation strategies. Elevating the curing temperature is an energy-consuming but effective solution for inhibiting efflorescence, which has been confirmed in many studies [111,113]. From the chemistry of raw materials' or reaction products' point of view, the inclusion of aluminates can lead to efflorescence reduction [113], which is attributed to the formation of more aluminate-incorporating gels that can fix more sodium ions. Additionally, by decreasing the  $\text{Na}_2\text{O}/\text{Al}_2\text{O}_3$  molar ratio in the mixture, efflorescence in geopolymers derived from metakaolin, biomass ash, and stone-cutting waste can be hindered [114]. Several hydrophobic additives such as calcite [115], silane crème [116,117], and calcium stearate [118] have also been proven beneficial in efflorescence mitigation.

However, some issues still need to be further understood. For instance, visual observation is the most regular approach so far, but it cannot provide a quantitative determination of the amount of efflorescence [33]. Moreover, the samples used to accelerate the efflorescence process are normally bottom-contacted with water, whereas it is insufficient to simulate the specimens serving in a real condition. Some recent works [115] indicate that assessing efflorescence in a climate chamber with wet–dry cycles might be closer to the practice.

#### 5.4. Carbonation

Carbonation of cementitious materials by atmospheric  $\text{CO}_2$  leads to a reduction in alkalinity in the pore solution and can further increase the vulnerability to corrosion of steel in concretes [119,120]. Due to the different chemistry involved, the carbonation mechanisms between portland cement materials and AAMs have some discrepancies. In a cement system, the atmospheric  $\text{CO}_2$  enters the pore solution and then immediately interacts with portlandite to the formation of  $\text{CaCO}_3$  [121]. Mild carbonation even enables to decrease in the porosity owing to the expansion of  $\text{CaCO}_3$  formation. In an AAM system, by contrast, the concentration of Ca in the pore solution is quite low and there is no portlandite existing as a buffer [122]. The carbonation takes place first in the pore solution and then in the C-N-A-S-H gels in an AAS system [122], leaving siliceous gels in addition to calcium carbonate. The siliceous gels can hardly contribute to the strength of the matrix. Hence, it appears that the AAM is more susceptible to carbonation than portland cement materials.

Nedeljković [123] investigated the carbonation mechanism of alkali-activated slag and fly ash pastes and found that the carbonation was enhanced with the increased dosage of slag, independent of the curing conditions. Moreover, the unsealed samples during curing showed poorer carbonation resistance than those cured under sealed conditions. Bernal et al. [122] studied the effect of metakaolin of AAS pastes on the resistance to carbonation. They found a 40–50% decrease in the compressive strength of samples upon full carbonation. A reduction in strength, a higher carbonation rate, and a larger capillary sorptivity of the binder were detected with the increase in metakaolin dosage. Shi et al. [124] explored the effect of alkali dosage and silicate modulus of AAS mortars under accelerated carbonation. The carbonation resistance of AAS mortars was found to increase with the increase in both the alkali dosage and silicate modulus. This is not only due to the higher alkalinity of the pore solution and higher reaction degree of slag, but also a reduced pore

size and porosity. Additionally, they assume that the carbonation of katoite enables an increase in the compressive strength of NaOH-based mortars.

Regarding the approach to enhance the carbonation resistance, Susan et al. [125] studied the effect of MgO content on the phase evolution and structural changes of AAS under accelerated carbonation. The gels and gismondine are the main reaction products formed in the AAS with a lower MgO, whereas in slags with a higher MgO content (5%) hydrotalcite was detected as the main secondary product to gels. Additionally, the AAS binder with a higher content of hydrotalcite was seemingly less sensitive to carbonation exposure, since hydrotalcite can act as an internal CO<sub>2</sub> sorbent in the matrix [125]. Future studies are recommended to further explore mitigating strategies of carbonation. In addition, the mechanism behind the reduced mechanical properties upon carbonation also requires more research, because it is still unclear whether the strength loss is because of the decalcification of the gels that happens on a microscale, or the development of microcracking due to drying/carbonation shrinkage that happens in meso scale (as we mentioned also in Section 5.1).

### 5.5. Alkali–Silica Reaction

AAMs commonly involve a high concentration of alkalis in their mixture design, thus it is spontaneously suspected that AAMs may suffer from alkali–silica reaction (ASR). The ASR occurs between hydroxyl ions in the pore solution and active Si in aggregates, including a series of progressive chemical reactions: (1) dissolution of active Si, (2) formation and gelation of nano-colloidal silica sol, (3) swelling of gels [126]. The formation of ASR products can result in the expansion or even cracking of the structure, to which significant attention should be paid. Earlier publications [127–130] indicate that ASR is not typically a severe problem for AAS materials which shows even better performance than portland cement system under accelerated ASR measurement. Despite this, some research assumed that AAS concrete is more vulnerable to alkali–aggregate reactions [131]. Therefore, there seems no consensus yet on whether ASR is a serious risk for the application of AAS concrete.

In recent years, some researchers devoted their efforts to exploring the influential factors of ASR in AAMs. For example, Chen et al. [132] studied the effect of the type of activators on the ASR expansion of AAS mortars. The rank of expansion is as follows: sodium silicate > sodium carbonate > sodium sulfate > sodium hydroxide. Shi et al. [133] investigated the influence of alkali dosage in sodium hydroxide-activated slag mortars on the resistance to ASR. The expansion induced by ASR decreases with the increase in alkali dosage as well as the pore solution alkalinity. A related work focused on the effect of silicate modulus on the ASR of AAS mortars was also carried out [134]. At the same high level of silicate modulus (1.5 and 2.0), the expansion of ASR tends to increase with the increase in alkali dosage, while it decreases with the increase in alkali dosage at a relatively lower silicate modulus (0 and 0.5).

Mitigation of ASR in AAMs is crucial for the sustainability of constructions. It is well known that supplementary cementitious materials with a high aluminum content, such as fly ash and metakaolin, can reduce ASR in the portland cement system [126,135]. A plausible reason is that a higher Al concentration in the pore solution can hinder the dissolution of active Si from aggregates. The addition of fly ash and metakaolin is confirmed to be also effective in AAS mortars. A 30% substitution of slag with fly ash has been proven to be an optimum amount to control ASR expansion [126]. Meanwhile, an increased dosage of metakaolin is conducive to suppressing ASR expansion in AAS, which can be completely inhibited when 70% of slag is replaced.

### 5.6. Chloride Ingress

The results showed that the chloride ion resistance of AAS systems is better than that of the cement mortar [136]. The improved ASTM C1202 method [137] is considered more suitable for the evaluation of chloride ion permeability of AAS mortar since it could effectively solve the problem of long immersion times. The critical content of chloride ions

in the AAS-based mortar (0.5 wt%) that causes the steel to passivate is significantly higher than that of PC mortar (0.3 wt%). AAS mortar exhibited a stronger ability to protect steel bars from corrosion than cement mortar due to its density and resistance to ion penetration. Monticelli [138] studied the corrosion protection afforded to the embedded rebar by AAFA mortar and found that AAFA provided lower corrosion protection to the rebar than PC mortar, probably due to the fast carbonation of AAFA so that de-passivation of the rebar occurred concurrently, despite a limited total chloride content inside the mortar. Through electrochemical experiments, Babaei found that the conventional classifications that are commonly used to assess the severity of corrosion in portland cement-based systems might need some recalibration to be used for low-calcium fly ash-based corroding systems [139]. Compared with rapid testing methods, chloride diffusion tests can better reflect the real chloride resistance of AAMs according to [140]. This review [140] also shows that the properties of precursors and activators all have effects on the chloride transport in AAMs. However, in general, the chloride resistance of AAMs is comparable to that of PC.

Different strategies are proposed to improve the chloride resistance of AAMs. Some admixtures like silica fume and nanoparticles can refine the pore structure of AAMs thus mitigating the chloride transport [141,142]. From the chemical absorption point of view, the addition of MgO, LDHs, and CLDHs is beneficial since they can absorb  $\text{Cl}^-$ , thus hindering the chloride ingress to the steel [143,144].

### 5.7. Other Issues

The resistance of AAMs to sulfate [145] and phosphoric acid [146] seems to be superior compared to PC. However, the information on the freeze and thaw resistance of AAMs seems controversial. Some studies identified very low freeze–thaw damage of AAS concrete [147], while other studies reported the opposite [148]. While the reasons behind this have not been confirmed yet, it is clear that in addition to the parameters of the raw materials, the curing and experimental conditions all significantly affect the test outcomes [149]. The experimental results obtained from different labs are hard to interpret or compare before a consistent protocol is used. Moreover, the effect of pre-conditioning, which is normally in drying conditions that can cause microcracking [101], on the freeze and thaw resistance of samples requires further research attention.

## 6. Concluding Remarks

In this paper, a current state-of-the-art review of AAMs is provided. Influential factors of the properties of AAMs are discussed. Commonly used characterization methods for AAMs are summarized. Challenges and future trends in the research field of AAMs are discussed. The following conclusions are obtained:

The properties of AAMs are influenced by various parameters including the chemical composition and particle size of the raw materials, composition of the activator, and curing conditions, among which the calcium content in the raw materials and the silicate content in the activator seem to govern the type and properties of the reaction products.

Many techniques that have shown their functions for portland cement can be applied in AAMs, but with individual limitations, such as the incapability of XRD in detecting nano-sized crystals and the difficulty in distinguishing C-A-S-H gels and carbonate phases using TG. In a combination of different techniques, they can counterbalance the disadvantages of each other.

Some properties of AAMs are superior to PC-based materials, while some are not. The shrinkage of AAMs under either sealed or exposed conditions is usually larger than that of PC, and drying-induced cracking may be aggravated by the co-occurrence of other effects like carbonation and efflorescence. Future research to decouple different degradation mechanisms is required to enhance the durability of AAMs.

**Author Contributions:** L.F.: Writing—original draft, Formal analysis; S.Y.: Writing—original draft, visualization; S.Z.: Investigation, visualization; Q.Z.: Investigation, visualization; F.R.: Investigation, visualization; C.L.: Writing—original draft, Writing—review & editing; Y.Z.: Writing—original

draft, Writing—review & editing; W.W.: Supervision, Writing—review & editing; N.X.: Supervision, Writing—review & editing; Z.L.: Methodology, Writing—original draft, Writing—review & editing; N.C.: Methodology, Supervision. All authors have read and agreed to the published version of the manuscript.

**Funding:** This research was funded by the Youth Innovation Support Program of Shandong Colleges and Universities, National Natural Science Foundation of China Regional Innovation and Development Joint Fund (U22A20126 and 52372026), Horizon Europe Guarantee Fund (Grant No. EP/X022587/1), Taishan Scholar Program, Case-by-Case Project for Top Outstanding Talents of Jinan, Double Hundred Foreign Expert Program (WST2018011), Jiangsu Industry-University-Research Corporation Program (BY2022254), Lianyungang Key Technique Competition Program (CGJBGS2103), and Lianyungang Science and Technology Transformation Program (CA202206).

**Data Availability Statement:** Some or all data, models, or code that support the findings of this study are available from the corresponding author upon reasonable request. The data are not publicly available due to privacy.

**Conflicts of Interest:** The authors declare no conflicts of interest.

## References

1. Kuhl, H. *Chemistry of Cement*; Band III; VerlagTechnik: Berlin, Germany, 1958. (In German)
2. Valente, M.; Sambucci, M.; Chougan, M.; Ghaffar, S.H. Reducing the emission of climate-altering substances in cementitious materials: A comparison between alkali-activated materials and Portland cement-based composites incorporating recycled tire rubber. *J. Clean. Prod.* **2022**, *333*, 130013. [[CrossRef](#)]
3. Luo, Y.; Klima, K.M.; Brouwers, H.J.H.; Yu, Q. Effects of ladle slag on Class F fly ash geopolymer: Reaction mechanism and high temperature behavior. *Cem. Concr. Compos.* **2022**, *129*, 104468. [[CrossRef](#)]
4. Oh, J.E.; Moon, J.; Oh, S.-G.; Clark, S.M.; Monteiro, P.J.M. Microstructural and compositional change of NaOH-activated high calcium fly ash by incorporating Na-aluminate and co-existence of geopolymeric gel and C-S-H(I). *Cem. Concr. Res.* **2012**, *42*, 673–685. [[CrossRef](#)]
5. Alnahhal, M.F.; Kim, T.; Hajimohammadi, A. Waste-derived activators for alkali-activated materials: A review. *Cem. Concr. Compos.* **2021**, *118*, 103980. [[CrossRef](#)]
6. Lee, W.K.W.; Van Deventer, J.S.J. The effect of ionic contaminants on the early-age properties of alkali-activated fly ash-based cements. *Cem. Concr. Res.* **2002**, *32*, 577–584. [[CrossRef](#)]
7. Gomes, K.C.; Carvalho, M.; Diniz, D.D.P.; Abrantes, R.D.C.C.; Branco, M.A.; Carvalho Junior, P.R.O.D. Carbon emissions associated with two types of foundations: CP-II Portland cement-based composite vs. geopolymer concrete. *Matéria* **2019**, *24*, e12525. [[CrossRef](#)]
8. Rashad, A.M.; Bai, Y.; Basheer, P.A.M.; Collier, N.C.; Milestone, N.B. Chemical and mechanical stability of sodium sulfate activated slag after exposure to elevated temperature. *Cem. Concr. Res.* **2012**, *42*, 333–343. [[CrossRef](#)]
9. Klima, K.M.; Schollbach, K.; Brouwers, H.J.H.; Yu, Q. Thermal and fire resistance of Class F fly ash based geopolymers—A review. *Constr. Build. Mater.* **2022**, *323*, 126529. [[CrossRef](#)]
10. Li, Z.; Nedeljković, M.; Chen, B.; Ye, G. Mitigating the autogenous shrinkage of alkali-activated slag by metakaolin. *Cem. Concr. Res.* **2019**, *122*, 30–41. [[CrossRef](#)]
11. Longhi, M.A.; Zhang, Z.; Walkley, B.; Rodríguez, E.D.; Kirchheim, A.P. Strategies for control and mitigation of efflorescence in metakaolin-based geopolymers. *Cem. Concr. Res.* **2021**, *144*, 106431. [[CrossRef](#)]
12. Xu, H.; Van Deventer, J.S.J. The geopolymerisation of alumino-silicate minerals. *Int. J. Miner. Process.* **2000**, *59*, 247–266. [[CrossRef](#)]
13. Xu, H.; Van Deventer, J.S.J. The effect of alkali metals on the formation of geopolymeric gels from alkali-feldspars. *Colloids Surf. A Physicochem. Eng. Asp.* **2003**, *216*, 27–44. [[CrossRef](#)]
14. Haha, M.B.; Lothenbach, B.; Le Saout, G.; Winnefeld, F. Influence of slag chemistry on the hydration of alkali-activated blast-furnace slag—Part I: Effect of MgO. *Cem. Concr. Res.* **2011**, *41*, 955–963. [[CrossRef](#)]
15. Yusuf, M.O.; Megat Johari, M.A.; Ahmad, Z.A.; Maslehuddin, M. Strength and microstructure of alkali-activated binary blended binder containing palm oil fuel ash and ground blast-furnace slag. *Constr. Build. Mater.* **2014**, *52*, 504–510. [[CrossRef](#)]
16. Cai, Y.; Liu, X. Mechanical properties test of pavement base or subbase made of solid waste stabilized by acetylene sludge and fly ash. *AIP Adv.* **2020**, *10*, 065022. [[CrossRef](#)]
17. Lu, C.; Zhang, Z.; Hu, J.; Yu, Q.; Shi, C. Effects of anionic species of activators on the rheological properties and early gel characteristics of alkali-activated slag paste. *Cem. Concr. Res.* **2022**, *162*, 106968. [[CrossRef](#)]
18. Lima, F.S.; Gomes, T.C.F.; Moraes, J.C.B. Effect of coffee husk ash as alkaline activator in one-part alkali-activated binder. *Constr. Build. Mater.* **2023**, *362*, 129799. [[CrossRef](#)]
19. Kalina, L.; Bílek, V.; Novotný, R.; Mončeková, M.; Másilko, J.; Koplík, J. Effect of Na<sub>3</sub>PO<sub>4</sub> on the Hydration Process of Alkali-Activated Blast Furnace Slag. *Materials* **2016**, *9*, 395. [[CrossRef](#)]

20. Lima, V.M.E.; Basto, P.A.; Henrique, M.A.; Almeida, Y.M.; de Melo Neto, A.A. Optimizing the concentration of Na<sub>2</sub>O in alkaline activators to improve mechanical properties and reduce costs and CO<sub>2</sub> emissions in alkali-activated mixtures. *Constr. Build. Mater.* **2022**, *344*, 128185. [[CrossRef](#)]
21. Collins, F.; Sanjayan, J.G. Early Age Strength and Workability of Slag Pastes Activated by NaOH and Na<sub>2</sub>CO<sub>3</sub>. *Cem. Concr. Res.* **1998**, *28*, 655–664. [[CrossRef](#)]
22. Walkley, B.; San Nicolas, R.; Sani, M.-A.; Bernal, S.A.; Van Deventer, J.S.J.; Provis, J.L. Structural evolution of synthetic alkali-activated CaO-MgO-Na<sub>2</sub>O-Al<sub>2</sub>O<sub>3</sub>-SiO<sub>2</sub> materials is influenced by Mg content. *Cem. Concr. Res.* **2017**, *99*, 155–171. [[CrossRef](#)]
23. Gómez-Casero, M.A.; Pérez-Villarejo, L.; Castro, E.; Eliche-Quesada, D. Effect of steel slag and curing temperature on the improvement in technological properties of biomass bottom ash based alkali-activated materials. *Constr. Build. Mater.* **2021**, *302*, 124205. [[CrossRef](#)]
24. Samantasinghar, S.; Singh, S. Effects of curing environment on strength and microstructure of alkali-activated fly ash-slag binder. *Constr. Build. Mater.* **2020**, *235*, 117481. [[CrossRef](#)]
25. Jittin, V.; Madhuri, P.; Santhanam, M.; Bahurudeen, A. Influence of preconditioning and curing methods on the durability performance of alkali-activated binder composites. *Constr. Build. Mater.* **2021**, *311*, 125346. [[CrossRef](#)]
26. Rashad, A.M. A comprehensive overview about the influence of different additives on the properties of alkali-activated slag—A guide for Civil Engineer. *Constr. Build. Mater.* **2013**, *47*, 29–55. [[CrossRef](#)]
27. Duxson, P.; Provis, J.L.; Lukey, G.C.; Mallicoat, S.W.; Kriven, W.M.; Van Deventer, J.S.J. Understanding the relationship between geopolymer composition, microstructure and mechanical properties. *Colloids Surf. A Physicochem. Eng. Asp.* **2005**, *269*, 47–58. [[CrossRef](#)]
28. Wang, Y.S.; Alrefaei, Y.; Dai, J.G. Silico-aluminophosphate and alkali-aluminosilicate geopolymers: A comparative review. *Front. Mater.* **2019**, *6*, 106. [[CrossRef](#)]
29. Wang, X.; Li, T.; Xie, W.; Zhang, L.; Li, D.; Xing, F. Molecular dynamics study on the structure and mechanical properties of tobermorite. *Mater. Sci. Eng. B* **2024**, *299*, 116930. [[CrossRef](#)]
30. Zhuang, X.Y.; Chen, L.; Komarneni, S.; Zhou, C.H.; Tong, D.S.; Yang, H.M.; Yu, W.H.; Wang, H. Fly ash-based geopolymer: Clean production, properties and applications. *J. Clean. Prod.* **2016**, *125*, 253–267. [[CrossRef](#)]
31. Fernández-Jiménez, A.; Palomo, A. Composition and microstructure of alkali activated fly ash binder: Effect of the activator. *Cem. Concr. Res.* **2005**, *35*, 1984–1992. [[CrossRef](#)]
32. Wang, Y.; Liu, X.; Tang, B.; Li, Y.; Zhang, W.; Xue, Y. Effect of Ca/(Si + Al) on red mud based eco-friendly revetment block: Microstructure, durability and environmental performance. *Constr. Build. Mater.* **2021**, *304*, 124618. [[CrossRef](#)]
33. Wang, Y.; Liu, X.; Zhang, W.; Li, Z.; Zhang, Y.; Li, Y.; Ren, Y. Effects of Si/Al ratio on the efflorescence and properties of fly ash based geopolymer. *J. Clean. Prod.* **2020**, *244*, 118852. [[CrossRef](#)]
34. Zhu, X.; Li, W.; Du, Z.; Zhou, S.; Zhang, Y.; Li, F. Recycling and utilization assessment of steel slag in metakaolin based geopolymer from steel slag by-product to green geopolymer. *Constr. Build. Mater.* **2021**, *305*, 124654. [[CrossRef](#)]
35. Puligilla, S.; Mondal, P. Role of slag in microstructural development and hardening of fly ash-slag geopolymer. *Cem. Concr. Res.* **2013**, *43*, 70–80. [[CrossRef](#)]
36. Puertas, F.; Torres-Carrasco, M. Use of glass waste as an activator in the preparation of alkali-activated slag. Mechanical strength and paste characterisation. *Cem. Concr. Res.* **2014**, *57*, 95–104. [[CrossRef](#)]
37. Jeon, D.; Jun, Y.; Jeong, Y.; Oh, J.E. Microstructural and strength improvements through the use of Na<sub>2</sub>CO<sub>3</sub> in a cementless Ca(OH)<sub>2</sub>-activated Class F fly ash system. *Cem. Concr. Res.* **2015**, *67*, 215–225. [[CrossRef](#)]
38. Kim, M.S.; Jun, Y.; Lee, C.; Oh, J.E. Use of CaO as an activator for producing a price-competitive non-cement structural binder using ground granulated blast furnace slag. *Cem. Concr. Res.* **2013**, *54*, 208–214. [[CrossRef](#)]
39. Burciaga-Díaz, O.; Betancourt-Castillo, I. Characterization of novel blast-furnace slag cement pastes and mortars activated with a reactive mixture of MgO-NaOH. *Cem. Concr. Res.* **2018**, *105*, 54–63. [[CrossRef](#)]
40. Wang, Q.; Sun, S.; Yao, G.; Wang, Z.; Lyu, X. Preparation and characterization of an alkali-activated cementitious material with blast-furnace slag, soda sludge, and industrial gypsum. *Constr. Build. Mater.* **2022**, *340*, 127735. [[CrossRef](#)]
41. Sun, K.; Ali, H.A.; Xuan, D.; Ban, J.; Poon, C.S. Utilization of APC residues from sewage sludge incineration process as activator of alkali-activated slag/glass powder material. *Cem. Concr. Compos.* **2022**, *133*, 104680. [[CrossRef](#)]
42. Alnahhal, M.F.; Hamdan, A.; Hajimohammadi, A.; Kim, T. Effect of rice husk ash-derived activator on the structural build-up of alkali activated materials. *Cem. Concr. Res.* **2021**, *150*, 106590. [[CrossRef](#)]
43. Somaratna, J.; Ravikumar, D.; Neithalath, N. Response of alkali activated fly ash mortars to microwave curing. *Cem. Concr. Res.* **2010**, *40*, 1688–1696. [[CrossRef](#)]
44. Nedeljković, M.; Ghiassi, B.; Van Der Laan, S.; Li, Z.; Ye, G. Effect of curing conditions on the pore solution and carbonation resistance of alkali-activated fly ash and slag pastes. *Cem. Concr. Res.* **2019**, *116*, 146–158. [[CrossRef](#)]
45. Pascual, A.B.; Tognonvi, T.M.; Tagnit-Hamou, A. Optimization study of waste glass powder-based alkali activated materials incorporating metakaolin: Activation and curing conditions. *J. Clean. Prod.* **2021**, *308*, 127435. [[CrossRef](#)]
46. González-García, D.M.; Téllez-Jurado, L.; Jiménez-Álvarez, F.J.; Balmori-Ramírez, H. Structural study of geopolymers obtained from alkali-activated natural pozzolan feldspars. *Ceram. Int.* **2017**, *43*, 2606–2613. [[CrossRef](#)]
47. Li, Z.; Zhang, S.; Zuo, Y.; Chen, W.; Ye, G. Chemical deformation of metakaolin based geopolymer. *Cem. Concr. Res.* **2019**, *120*, 108–118. [[CrossRef](#)]

48. Khan, M.S.H.; Kayali, O.; Troitzsch, U. Effect of NaOH activation on sulphate resistance of GGBFS and binary blend pastes. *Cem. Concr. Compos.* **2017**, *81*, 49–58. [[CrossRef](#)]
49. Garcia-Lodeiro, I.; Palomo, A.; Fernández-Jiménez, A.; Macphee, D.E. Compatibility studies between NASH and CASH gels. Study in the ternary diagram  $\text{Na}_2\text{O}-\text{CaO}-\text{Al}_2\text{O}_3-\text{SiO}_2-\text{H}_2\text{O}$ . *Cem. Concr. Res.* **2011**, *41*, 923–931. [[CrossRef](#)]
50. Bernal, S.A.; Provis, J.L.; Walkley, B.; San Nicolas, R.; Gehman, J.D.; Brice, D.G.; Kilcullen, A.R.; Duxson, P.; Van Deventer, J.S.J. Gel nanostructure in alkali-activated binders based on slag and fly ash, and effects of accelerated carbonation. *Cem. Concr. Res.* **2013**, *53*, 127–144. [[CrossRef](#)]
51. Sun, Z.; Lin, X.; Liu, P.; Wang, D.; Vollpracht, A.; Oeser, M. Study of alkali activated slag as alternative pavement binder. *Constr. Build. Mater.* **2018**, *186*, 626–634. [[CrossRef](#)]
52. Williams, R.P.; Hart, R.D.; Van Riessen, A. Quantification of the Extent of Reaction of Metakaolin-Based Geopolymers Using X-Ray Diffraction, Scanning Electron Microscopy, and Energy-Dispersive Spectroscopy. *J. Am. Ceram. Soc.* **2011**, *94*, 2663–2670. [[CrossRef](#)]
53. Li, Z.; Lu, T.; Liang, X.; Dong, H.; Ye, G. Mechanisms of autogenous shrinkage of alkali-activated slag and fly ash pastes. *Cem. Concr. Res.* **2020**, *135*, 106107. [[CrossRef](#)]
54. Provis, J.L.; Lukey, G.C.; Van Deventer, J.S.J. Do Geopolymers Actually Contain Nanocrystalline Zeolites? A Reexamination of Existing Results. *Chem. Mater.* **2005**, *17*, 3075–3085. [[CrossRef](#)]
55. Uysal, M.; Aygörmec, Y.; Canpolat, O.; Cosgun, T.; Faruk Kuranlı, Ö. Investigation of using waste marble powder, brick powder, ceramic powder, glass powder, and rice husk ash as eco-friendly aggregate in sustainable red mud-metakaolin based geopolymer composites. *Constr. Build. Mater.* **2022**, *361*, 129718. [[CrossRef](#)]
56. Zhang, Y.; Saravanakumar, K.; Çopuroğlu, O. EDS Microanalysis of Unhydrated Blast Furnace Slag Grains in Field Concrete with Different Service Life. *Microsc. Microanal.* **2022**, *28*, 1493–1503. [[CrossRef](#)]
57. Ma, Y.; Wang, G.; Ye, G.; Hu, J. A comparative study on the pore structure of alkali-activated fly ash evaluated by mercury intrusion porosimetry, N-2 adsorption and image analysis. *J. Mater. Sci.* **2018**, *53*, 5958–5972. [[CrossRef](#)]
58. Ismail, I.; Bernal, S.A.; Provis, J.L.; San Nicolas, R.; Hamdan, S.; Van Deventer, J.S.J. Modification of phase evolution in alkali-activated blast furnace slag by the incorporation of fly ash. *Cem. Concr. Compos.* **2014**, *45*, 125–135. [[CrossRef](#)]
59. Aliques-Granero, J.; Tognonvi, M.T.; Tagnit-Hamou, A. Durability study of AAMs: Sulfate attack resistance. *Constr. Build. Mater.* **2019**, *229*, 117100. [[CrossRef](#)]
60. Bernal, S.A.; Provis, J.L.; Green, D.J. Durability of Alkali-Activated Materials: Progress and Perspectives. *J. Am. Ceram. Soc.* **2014**, *97*, 997–1008. [[CrossRef](#)]
61. Goldstein, J.I.; Newbury, D.E.; Michael, J.R.; Ritchie, N.W.; Scott, J.H.J.; Joy, D.C. Quantitative analysis: From k-ratio to composition. In *Scanning Electron Microscopy and X-ray Microanalysis*; Springer: Berlin/Heidelberg, Germany, 2018; pp. 289–307.
62. Ye, H.; Cai, R.; Tian, Z. Natural carbonation-induced phase and molecular evolution of alkali-activated slag: Effect of activator composition and curing temperature. *Constr. Build. Mater.* **2020**, *248*, 118726. [[CrossRef](#)]
63. Scrivener, K.; Snellings, R.; Lothenbach, B. *A Practical Guide to Microstructural Analysis of Cementitious Materials*; CRC Press: Boca Raton, FL, USA, 2016.
64. Justnes, H.; Meland, I.; Bjoergum, J.O.; Krane, J.; Skjetne, T. Nuclear magnetic resonance (NMR)—A powerful tool in cement and concrete research. *Adv. Cem. Res.* **1990**, *3*, 105–110. [[CrossRef](#)]
65. Schöler, A.; Winnefeld, F.; Haha, M.B.; Lothenbach, B. The effect of glass composition on the reactivity of synthetic glasses. *J. Am. Ceram. Soc.* **2017**, *100*, 2553–2567. [[CrossRef](#)]
66. Myers, R.J.; Bernal, S.A.; Gehman, J.D.; Van Deventer, J.S.J.; Provis, J.L.; Struble, L. The Role of Al in Cross-Linking of Alkali-Activated Slag Cements. *J. Am. Ceram. Soc.* **2015**, *98*, 996–1004. [[CrossRef](#)]
67. Sevelsted, T.F.; Skibsted, J. Carbonation of C-S-H and C-A-S-H samples studied by  $^{13}\text{C}$ ,  $^{27}\text{Al}$  and  $^{29}\text{Si}$  MAS NMR spectroscopy. *Cem. Concr. Res.* **2015**, *71*, 56–65. [[CrossRef](#)]
68. Wang, Y.; Cao, Y.; Zhang, Z.; Huang, J.; Zhang, P.; Ma, Y.; Wang, H. Study of acidic degradation of alkali-activated materials using synthetic C-(N)-A-S-H and N-A-S-H gels. *Compos. Part B Eng.* **2022**, *230*, 109510. [[CrossRef](#)]
69. Siddique, S.; Jang, J.G. Acid and sulfate resistance of seawater based alkali activated fly ash: A sustainable and durable approach. *Constr. Build. Mater.* **2021**, *281*, 122601. [[CrossRef](#)]
70. Longhi, M.A.; Rodríguez, E.D.; Walkley, B.; Eckhard, D.; Zhang, Z.; Provis, J.L.; Kirchheim, A.P. Metakaolin-based geopolymers: Efflorescence and its effect on microstructure and mechanical properties. *Ceram. Int.* **2022**, *48*, 2212–2229. [[CrossRef](#)]
71. Gong, K.; White, C.E. Impact of chemical variability of ground granulated blast-furnace slag on the phase formation in alkali-activated slag pastes. *Cem. Concr. Res.* **2016**, *89*, 310–319. [[CrossRef](#)]
72. White, C.E.; Page, K.; Henson, N.J.; Provis, J.L. In situ synchrotron X-ray pair distribution function analysis of the early stages of gel formation in metakaolin-based geopolymers. *Appl. Clay Sci.* **2013**, *73*, 17–25. [[CrossRef](#)]
73. White, C.E.; Provis, J.L.; Llobet, A.; Proffen, T.; van Deventer, J.S.J. Evolution of Local Structure in Geopolymer Gels: An In Situ Neutron Pair Distribution Function Analysis. *J. Am. Ceram. Soc.* **2011**, *94*, 3532–3539. [[CrossRef](#)]
74. Shi, D.; Ye, J.; Zhang, W.; Shen, W. Properties, mineralogy and microstructure evolution of 4-year calcium silicate slag-based alkali-activated materials. *Cem. Concr. Compos.* **2023**, *136*, 104857. [[CrossRef](#)]
75. Li, J.; Li, J.; Wei, H.; Yang, X.; Benoit, G.; Jiao, X. Alkaline-thermal activated electrolytic manganese residue-based geopolymers for efficient immobilization of heavy metals. *Constr. Build. Mater.* **2021**, *298*, 123853. [[CrossRef](#)]

76. Zhang, B.; Yu, T.; Deng, L.; Li, Y.; Guo, H.; Zhou, J.; Li, L.; Peng, Y. Ion-adsorption type rare earth tailings for preparation of alkali-based geopolymer with capacity for heavy metals immobilization. *Cem. Concr. Compos.* **2022**, *134*, 104768. [[CrossRef](#)]
77. Jain, S.; Banthia, N.; Troczynski, T. Leaching of immobilized cesium from NaOH-activated fly ash-based geopolymers. *Cem. Concr. Compos.* **2022**, *133*, 104679. [[CrossRef](#)]
78. Shi, C.; Fernández-Jiménez, A. Stabilization/solidification of hazardous and radioactive wastes with alkali-activated cements. *J. Hazard. Mater.* **2006**, *137*, 1656–1663. [[CrossRef](#)]
79. Mobasher, N.; Bernal, S.A.; Kinoshita, H.; Sharrad, C.A.; Provis, J.L. Gamma irradiation resistance of an early age slag-blended cement matrix for nuclear waste encapsulation. *J. Mater. Res.* **2015**, *30*, 1563–1571. [[CrossRef](#)]
80. Ye, H. *Mechanisms and Mitigation of Shrinkage in Alkali-Activated Slag*; The Pennsylvania State University: State College, PA, USA, 2016.
81. Uppalapati, S.; Cizer, Ö. Assessing the autogenous shrinkage of alkali-activated slag/fly ash mortar blends. *Am. Concr. Inst. ACI Spec. Publ.* **2017**, *320*, 1–12.
82. Chen, W.; Li, B.; Wang, J.; Thom, N. Effects of alkali dosage and silicate modulus on autogenous shrinkage of alkali-activated slag cement paste. *Cem. Concr. Res.* **2021**, *141*, 106322. [[CrossRef](#)]
83. Uppalapati, S.; Vandewalle, L.; Cizer, Ö. Autogenous shrinkage of slag-fly ash blends activated with hybrid sodium silicate and sodium sulfate at different curing temperatures. *Constr. Build. Mater.* **2020**, *265*, 121276. [[CrossRef](#)]
84. Nedeljković, M.; Li, Z.; Ye, G. Setting, Strength, and Autogenous Shrinkage of Alkali-Activated Fly Ash and Slag Pastes: Effect of Slag Content. *Materials* **2018**, *11*, 2121. [[CrossRef](#)]
85. Uppalapati, S. *Early-Age Structural Development and Autogenous Shrinkage of Alkali-Activated Slag/Fly-Ash Cements*; KU Leuven: Leuven, Belgium, 2021.
86. Davidovits, J. *Geopolymer Cement. A Review*; Geopolymer Institute: Saint-Quentin, France, 2013; Volume 21, pp. 1–11.
87. Wallah, S. Drying Shrinkage of Heat-Cured Fly Ash-Based Geopolymer Concrete. *Mod. Appl. Sci.* **2009**, *3*, 14–21. [[CrossRef](#)]
88. Hu, Z.; Wyrzykowski, M.; Lura, P. Estimation of reaction kinetics of geopolymers at early ages. *Cem. Concr. Res.* **2020**, *129*, 105971. [[CrossRef](#)]
89. Li, Z.; Lu, T.; Chen, Y.; Wu, B.; Ye, G. Prediction of the autogenous shrinkage and microcracking of alkali-activated slag and fly ash concrete. *Cem. Concr. Compos.* **2021**, *117*, 103913. [[CrossRef](#)]
90. Palacios, M.; Puertas, F. Effect of shrinkage-reducing admixtures on the properties of alkali-activated slag mortars and pastes. *Cem. Concr. Res.* **2007**, *37*, 691–702. [[CrossRef](#)]
91. Kalina, L.; Bílek, V.; Bartoničková, E.; Krouska, J. Polypropylene Glycols as Effective Shrinkage-Reducing Admixtures in Alkali-Activated Materials. *ACI Mater. J.* **2018**, *115*, 251. [[CrossRef](#)]
92. Bílek, V., Jr.; Kalina, L.; Fojtík, O. *Shrinkage-Reducing Admixture Efficiency in Alkali-Activated Slag across the Different Doses of Activator*; *Proceedings of the Key Engineering Materials*; Trans Tech Publications: Zurich, Switzerland, 2018.
93. Qu, Z.Y.; Yu, Q.; Ji, Y.D.; Gauvin, F.; Voets, I.K. Mitigating shrinkage of alkali activated slag with biofilm. *Cem. Concr. Res.* **2020**, *138*, 106234. [[CrossRef](#)]
94. Li, Z.; Wyrzykowski, M.; Dong, H.; Granja, J.; Azenha, M.; Lura, P.; Ye, G. Internal curing by superabsorbent polymers in alkali-activated slag. *Cem. Concr. Res.* **2020**, *135*, 106123. [[CrossRef](#)]
95. Vafaei, B.; Farzarian, K.; Ghahremaninezhad, A. The influence of superabsorbent polymer on the properties of alkali-activated slag pastes. *Constr. Build. Mater.* **2020**, *236*, 117525. [[CrossRef](#)]
96. Ballekere Kumarappa, D.; Peethamparan, S.; Ngami, M. Autogenous shrinkage of alkali activated slag mortars: Basic mechanisms and mitigation methods. *Cem. Concr. Res.* **2018**, *109*, 1–9. [[CrossRef](#)]
97. Zhang, G.-Z.; Lee, H.-S.; Wang, X.-Y.; Han, Y. Internal Curing Effect of Pre-Soaked Zeolite Sand on the Performance of Alkali-Activated Slag. *Materials* **2021**, *14*, 718. [[CrossRef](#)]
98. Huang, J.; Yan, J.; Liu, K.; Wei, B.; Zou, C. Influence of Cooking Oil on the Mitigation of Autogenous Shrinkage of Alkali-Activated Slag Concrete. *Materials* **2020**, *13*, 4907. [[CrossRef](#)] [[PubMed](#)]
99. Jensen, O.M.; Hansen, P.F. Autogenous deformation and RH-change in perspective. *Cem. Concr. Res.* **2001**, *31*, 1859–1865. [[CrossRef](#)]
100. Neville, A.M. *Properties of Concrete*; Longman: London, UK, 1995.
101. Li, Z.; Liu, J.; Ye, G. Drying shrinkage of alkali-activated slag and fly ash concrete; A comparative study with ordinary Portland cement concrete. *Heron* **2019**, *64*, 1–15.
102. Ye, H.; Huang, L. Degradation mechanisms of alkali-activated binders in sulfuric acid: The role of calcium and aluminum availability. *Constr. Build. Mater.* **2020**, *246*, 118477. [[CrossRef](#)]
103. Li, Z.; Zhang, S.; Liang, X.; Ye, G. Cracking potential of alkali-activated slag and fly ash concrete subjected to restrained autogenous shrinkage. *Cem. Concr. Compos.* **2020**, *114*, 103767. [[CrossRef](#)]
104. Prinsse, S.; Hordijk, D.A.; Ye, G.; Lagendijk, P.; Luković, M. Time-dependent material properties and reinforced beams behavior of two alkali-activated types of concrete. *Struct. Concr.* **2020**, *21*, 642–658. [[CrossRef](#)]
105. Li, Z.; Chen, Y.; Provis, J.L.; Cizer, Ö.; Ye, G. Autogenous shrinkage of alkali-activated slag: A critical review. *Cem. Concr. Res.* **2023**, *172*, 107244. [[CrossRef](#)]
106. Wallah, S.J. Creep behaviour of fly ash-based geopolymer concrete. *Civ. Eng. Dimens.* **2010**, *12*, 73–78.
107. Zhou, X.; Wang, Y.; Zheng, W.; Chen, P.; Zeng, Y. Effect of Stress–Strength Ratio on Creep Property of Sodium Silicate–Based Alkali-Activated Slag Concrete. *Appl. Sci.* **2019**, *9*, 3643. [[CrossRef](#)]
108. Davidovits, J. *Geopolymer Chemistry & Applications*, 4th ed.; Geopolymer Institute: Saint-Quentin, France, 2015.

109. Lyu, W. Effect of Micro-Cracking and Self-Healing on Long-Term Creep and Strength Development of Concrete. Ph.D. Thesis, Delft University of Technology, Delft, The Netherlands, 2020.
110. Škvára, F.; Kopecký, L.; Myšková, L.; Šmilauer, V.; Alberovská, L.; Vinšová, L. Aluminosilicate polymers—Influence of elevated temperatures, efflorescence. *Ceramics* **2009**, *53*, 276–282.
111. Zhang, Z.; Provis, J.L.; Reid, A.; Wang, H. Fly ash-based geopolymers: The relationship between composition, pore structure and efflorescence. *Cem. Concr. Res.* **2014**, *64*, 30–41. [[CrossRef](#)]
112. Zhang, Z.; Provis, J.L.; Ma, X.; Reid, A.; Wang, H. Efflorescence and subflorescence induced microstructural and mechanical evolution in fly ash-based geopolymers. *Cem. Concr. Compos.* **2018**, *92*, 165–177. [[CrossRef](#)]
113. Najafi Kani, E.; Allahverdi, A.; Provis, J.L. Efflorescence control in geopolymer binders based on natural pozzolan. *Cem. Concr. Compos.* **2012**, *34*, 25–33. [[CrossRef](#)]
114. Simão, L.; Fernandes, E.; Hotza, D.; Ribeiro, M.J.; Montedo, O.R.K.; Raupp-Pereira, F. Controlling efflorescence in geopolymers: A new approach. *Case Stud. Constr. Mater.* **2021**, *15*, e00740. [[CrossRef](#)]
115. Wu, B.; Ma, X.; Deng, H.; Li, Y.; Xiang, Y.; Zhu, Y. An efficient approach for mitigation of efflorescence in fly ash-based geopolymer mortars under high-low humidity cycles. *Constr. Build. Mater.* **2022**, *317*, 126159. [[CrossRef](#)]
116. Pasupathy, K.; Ramakrishnan, S.; Sanjayan, J. Effect of hydrophobic surface-modified fine aggregates on efflorescence control in geopolymer. *Cem. Concr. Compos.* **2022**, *126*, 104337. [[CrossRef](#)]
117. Xue, X.; Liu, Y.-L.; Dai, J.-G.; Poon, C.-S.; Zhang, W.-D.; Zhang, P. Inhibiting efflorescence formation on fly ash-based geopolymer via silane surface modification. *Cem. Concr. Compos.* **2018**, *94*, 43–52. [[CrossRef](#)]
118. Chindaprasirt, P.; Jitsangiam, P.; Rattanasak, U. Hydrophobicity and efflorescence of lightweight fly ash geopolymer incorporated with calcium stearate. *J. Clean. Prod.* **2022**, *364*, 132449. [[CrossRef](#)]
119. Sufian Badar, M.; Kupwade-Patil, K.; Bernal, S.A.; Provis, J.L.; Allouche, E.N. Corrosion of steel bars induced by accelerated carbonation in low and high calcium fly ash geopolymer concretes. *Constr. Build. Mater.* **2014**, *61*, 79–89. [[CrossRef](#)]
120. Criado, M.; Monticelli, C.; Fajardo, S.; Gelli, D.; Grassi, V.; Bastidas, J.M. Organic corrosion inhibitor mixtures for reinforcing steel embedded in carbonated alkali-activated fly ash mortar. *Constr. Build. Mater.* **2012**, *35*, 30–37. [[CrossRef](#)]
121. Morandau, A.; Thiéry, M.; Dangla, P. Investigation of the carbonation mechanism of CH and C-S-H in terms of kinetics, microstructure changes and moisture properties. *Cem. Concr. Res.* **2014**, *56*, 153–170. [[CrossRef](#)]
122. Bernal, S.A.; De Gutierrez, R.M.; Provis, J.L.; Rose, V. Effect of silicate modulus and metakaolin incorporation on the carbonation of alkali silicate-activated slags. *Cem. Concr. Res.* **2010**, *40*, 898–907. [[CrossRef](#)]
123. Nedeljković, M. Carbonation Mechanism of Alkali-Activated Fly Ash and Slag Materials. Ph.D. Thesis, Delft University of Technology, Delft, The Netherlands, 2019. [[CrossRef](#)]
124. Shi, Z.; Shi, C.; Wan, S.; Li, N.; Zhang, Z. Effect of alkali dosage and silicate modulus on carbonation of alkali-activated slag mortars. *Cem. Concr. Res.* **2018**, *113*, 55–64. [[CrossRef](#)]
125. Bernal, S.A.; San Nicolas, R.; Myers, R.J.; Mejía De Gutiérrez, R.; Puertas, F.; van Deventer, J.S.J.; Provis, J.L. MgO content of slag controls phase evolution and structural changes induced by accelerated carbonation in alkali-activated binders. *Cem. Concr. Res.* **2014**, *57*, 33–43. [[CrossRef](#)]
126. Rajabipour, F.; Giannini, E.; Dunant, C.; Ideker, J.H.; Thomas, M.D.A. Alkali-silica reaction: Current understanding of the reaction mechanisms and the knowledge gaps. *Cem. Concr. Res.* **2015**, *76*, 130–146. [[CrossRef](#)]
127. Gifford, P.M.; Gillott, J.E. Alkali-silica reaction (ASR) and alkali-carbonate reaction (ACR) in activated blast furnace slag cement (ABFSC) concrete. *Cem. Concr. Res.* **1996**, *26*, 21–26. [[CrossRef](#)]
128. Fernández-Jiménez, A.; Puertas, F. The alkali-silica reaction in alkali-activated granulated slag mortars with reactive aggregate. *Cem. Concr. Res.* **2002**, *32*, 1019–1024. [[CrossRef](#)]
129. Al-Otaibi, S. Durability of concrete incorporating GGBS activated by water-glass. *Constr. Build. Mater.* **2008**, *22*, 2059–2067. [[CrossRef](#)]
130. Puertas, F.; Palacios, M.; Gil-Maroto, A.; Vázquez, T. Alkali-aggregate behaviour of alkali-activated slag mortars: Effect of aggregate type. *Cem. Concr. Compos.* **2009**, *31*, 277–284. [[CrossRef](#)]
131. Cao, J.; Chung, D.D.L. Improving the dispersion of steel fibers in cement mortar by the addition of silane. *Cem. Concr. Res.* **2001**, *31*, 309–311. [[CrossRef](#)]
132. You-Zhi, C.; Xin-Cheng, P.; Chang-Hui, Y.; Qing-Jun, D. Alkali aggregate reaction in alkali slag cement mortars. *J. Wuhan Univ. Technol.-Mater. Sci. Ed.* **2002**, *17*, 60–62. [[CrossRef](#)]
133. Shi, Z.; Shi, C.; Wan, S.; Ou, Z. Effect of alkali dosage on alkali-silica reaction in sodium hydroxide activated slag mortars. *Constr. Build. Mater.* **2017**, *143*, 16–23. [[CrossRef](#)]
134. Shi, Z.; Shi, C.; Wan, S.; Zhang, Z. Effects of alkali dosage and silicate modulus on alkali-silica reaction in alkali-activated slag mortars. *Cem. Concr. Res.* **2018**, *111*, 104–115. [[CrossRef](#)]
135. Lindgård, J.; Andić-Çakır, Ö.; Fernandes, I.; Rønning, T.F.; Thomas, M.D.A. Alkali-silica reactions (ASR): Literature review on parameters influencing laboratory performance testing. *Cem. Concr. Res.* **2012**, *42*, 223–243. [[CrossRef](#)]
136. Liang, X.; Yin, S. Evaluation of the flexural behavior and serviceability of engineered cementitious composite-coral aggregate concrete beams reinforced with BFRP bars. *Constr. Build. Mater.* **2021**, *308*, 124937. [[CrossRef](#)]
137. ASTM C1202-19; Standard Test Method for Electrical Indication of Concrete's Ability to Resist Chloride Ion Penetration. ASTM International: West Conshohocken, PA, USA, 2022.

138. Monticelli, C.; Natali, M.E.; Balbo, A.; Chiavari, C.; Zanutto, F.; Manzi, S.; Bignozzi, M.C. A study on the corrosion of reinforcing bars in alkali-activated fly ash mortars under wet and dry exposures to chloride solutions. *Cem. Concr. Res.* **2016**, *87*, 53–63. [[CrossRef](#)]
139. Babaei, M.; Castel, A. Chloride-induced corrosion of reinforcement in low-calcium fly ash-based geopolymer concrete. *Cem. Concr. Res.* **2016**, *88*, 96–107. [[CrossRef](#)]
140. Zhang, J.; Ma, Y.; Hu, J.; Wang, H.; Zhang, Z. Review on chloride transport in alkali-activated materials: Role of precursors, activators and admixtures. *Constr. Build. Mater.* **2022**, *328*, 127081. [[CrossRef](#)]
141. Jena, S.; Panigrahi, R.; Sahu, P. Mechanical and Durability Properties of Fly Ash Geopolymer Concrete with Silica Fume. *J. Inst. Eng. Ser. A* **2019**, *100*, 697–705. [[CrossRef](#)]
142. Ramezani-pour, A.A.; Moeini, M.A. Mechanical and durability properties of alkali activated slag coating mortars containing nanosilica and silica fume. *Constr. Build. Mater.* **2018**, *163*, 611–621. [[CrossRef](#)]
143. Liu, T.; Chen, Y.; Yu, Q.; Fan, J.; Brouwers, H.J.H. Effect of MgO, Mg-Al-NO<sub>3</sub> LDH and calcined LDH-CO<sub>3</sub> on chloride resistance of alkali activated fly ash and slag blends. *Constr. Build. Mater.* **2020**, *250*, 118865. [[CrossRef](#)]
144. Yoon, H.N.; Park, S.M.; Lee, H.K. Effect of MgO on chloride penetration resistance of alkali-activated binder. *Constr. Build. Mater.* **2018**, *178*, 584–592. [[CrossRef](#)]
145. Van Rijswijk, T. Utilization of Alkali Activated Concrete in Concrete Revetment Products. Master's Thesis, Delft University of Technology, Delft, The Netherlands, 2022.
146. Ren, J.; Zhang, L.; Zhu, Y.; Li, Z.; San Nicolas, R. A Comparative Study on the Degradation of Alkali-Activated Slag/Fly Ash and Cement-Based Mortars in Phosphoric Acid. *Front. Mater.* **2022**, *9*, 845349. [[CrossRef](#)]
147. Fu, Y.; Cai, L.; Yonggen, W. Freeze–thaw cycle test and damage mechanics models of alkali-activated slag concrete. *Constr. Build. Mater.* **2011**, *25*, 3144–3148. [[CrossRef](#)]
148. Yang, Z.; Shi, P.; Zhang, Y.; Li, Z. Effect of superabsorbent polymer introduction on properties of alkali-activated slag mortar. *Constr. Build. Mater.* **2022**, *340*, 127541. [[CrossRef](#)]
149. Winnefeld, F.; Gluth, G.J.G.; Bernal, S.A.; Bignozzi, M.C.; Carabba, L.; Chithiraputhiran, S.; Dehghan, A.; Dolenc, S.; Dombrowski-Daube, K.; Dubey, A.; et al. RILEM TC 247-DTA round robin test: Sulfate resistance, alkali-silica reaction and freeze–thaw resistance of alkali-activated concretes. *Mater. Struct.* **2020**, *53*, 140. [[CrossRef](#)]

**Disclaimer/Publisher's Note:** The statements, opinions and data contained in all publications are solely those of the individual author(s) and contributor(s) and not of MDPI and/or the editor(s). MDPI and/or the editor(s) disclaim responsibility for any injury to people or property resulting from any ideas, methods, instructions or products referred to in the content.